This dissertation has been
microfilmed exactly as received 67-15,585

ANDERSON, Jr., Robert Morris, 1939-
THE EFFECT OF MECHANICAL STRESS UPON
RECTIFYING METAL-SEMICONDUCTOR CONTACTS.

The University of Michigan, Ph.D., 1967
Engineering, electrical

University Microfilms, Inc., Ann Arbor, Michigan

THE EFFECT OF MECHANICAL STRESS UPON RECTIFYING METAL-SEMICONDUCTOR CONTACTS

by

Robert Morris Anderson, Jr.

A dissertation submitted in partial fulfillment
of the requirements for the degree of
Doctor of Philosophy in The
University of Michigan
1967

Doctoral Committee:

Associate Professor Howard Diamond, Chairman
Professor Louis J. Cutrona
Professor Dale M. Grimes
Associate Professor George I. Haddad
Professor Gabriel Weinreich

EFFECT OF MECHANICAL STRESS ON RECTIFYING METAL-SEMICONDUCTOR CONTACTS

By Robert Morris Anderson, Jr.

The purpose of this study is to investigate the effects of mechanical stress on the electrical properties of metal-silicon rectifying contacts. The effect is well known, but has never been explained in terms of the physical mechanisms which are involved.

The theoretical electrical properties of an unstressed rectifying metal-semiconductor are considered. The various currents, i.e., Schottky, minority carrier, space-charge recombination and surface recombination, are considered and mathematical expressions for each are developed. Conditions are presented which allow a prediction of the volt-ampere characteristic of a general metal-semiconductor contact.

The stress dependence of the various quantities appearing in the above current expressions is discussed theoretically. Two major stress dependent mechanisms are presented. First, the electronic band structure of bulk silicon is discussed in terms of deformation potential theory. The linear decrease in the band gap with compressive strain is developed. The changes which occur in the band structure of the bulk are extrapolated to the surface of the crystal. This extrapolation yields a prediction of the strain dependence of the electronic

barrier height as a function of the type and direction of the stress, as well as the crystallographic orientation of the crystal. The other major mechanism is described as a stress dependent shift in the energy levels of trapping centers in the space charge region. It appears that the trap levels move toward the intrinsic level when compressional stress is applied. This has the effect of increasing the space charge generation-recombination current.

Experimental data are presented on small area, evaporated gold contacts on n-type silicon. (Details of the fabrication process are also included.) The zero stress volt-ampere characteristic is shown to be dominated by Schottky current. When compressional stress is applied to the contact by means of a stylus, the volt-ampere characteristic shifts in the direction of decreasing contact resistance. For an applied stress less than 3×10^9 dyne/cm^2, the change in the current in the reverse bias region and in the low forward bias region is much larger than the change in the high forward bias region.

The small change in the high forward bias range is shown to correlate with the expected change in the electronic barrier height. The large change in the reverse and low forward bias range is interpreted as a change in the space charge generation-recombination current component which results when the effective trap energy moves closer to the intrinsic energy.

Two conclusions can be drawn from this investigation. One, the stress dependence of the electronic barrier of a rectifying contact can be predicted on the basis of the stress dependence of the band gap of the semiconductor. Two, another, more sensitive, stress mechanism appears to be a stress dependent shift in the effective trap energy toward the intrinsic energy of the semiconductor.

ACKNOWLEDGEMENTS

The author wishes to express his gratitude to the following individuals and organizations for the part that each played in the successful conclusion of this investigation:

Howard Diamond for his suggestion of the problem and for his untiring support and encouragement and his expeditious reading and editing of the first draft of this dissertation;

The doctoral committee for many fruitful and stimulating discussions;

The Electro-Voice Corporation and the National Aeronautics and Space Administration, Goddard Space Flight Center (Contract No. NAS5-9113) for providing the financial support;

The staff of the Microelectronics Laboratory for fruitful discussions;

The Research Laboratory of Tecumseh Products Company for the use of their silicon laboratory facilities and in particular, Mr. Raymond Kennedy and Mr. Terry Martin for many useful discussions and for their unselfish disclosure of silicon processing techniques;

The Electronic Products Division of the Dow Corning Corporation and the Materials and Controls Division of Texas Instruments, Inc. for supplying the silicon material used;

Towne Laboratories for supplying the evaporation masks;

Janice P. Anderson, my wife, for her continuous support and encouragement throughout this investigation and particularly for her patience in the final phase.

TABLE OF CONTENTS

	Page
ACKNOWLEDGEMENTS	ii
LIST OF SYMBOLS	vi
LIST OF TABLES	xiii
LIST OF FIGURES	xiv
CHAPTER I: INTRODUCTION	1
CHAPTER II: RECTIFYING METAL-SEMICONDUCTOR CONTACTS	4
2.1 Formation of the Potential Barrier	4
2.2 Majority Carrier (Schottky) Barrier	14
2.3 Minority Carrier Current	16
2.4 Space-Charge Recombination Current	18
2.5 Surface Recombination Current	25
2.6 Summary	26
CHAPTER III: EFFECT OF MECHANICAL STRESS ON THE VOLT-AMPERE CHARACTERISTIC	28
3.1 Effect of Stress on the Energy Band Diagram of a Rectifying Contact	28
3.2 Stress Dependence of Majority Carrier (Schottky) Current	48
3.3 Stress Dependence of Minority Carrier Current	50
3.4 Stress Dependence of the Space-Charge Recombination Current	53
3.5 Stress Dependence of Surface Recombination Current	58
3.6 Summary	58
CHAPTER IV: EXPERIMENTAL RESULTS AND COMPARISON WITH THEORY	61
4.1 The Experimental Setup	61
4.2 Experimental Volt-Ampere Characteristic with Zero Mechanical Stress	68

Page

4.3 Experimental Volt-Ampere Characteristic with Mechanical Stress 78
4.4 Summary 88

CHAPTER V: SUMMARY AND CONCLUSIONS 89

APPENDIX A: STRESS STRAIN RELATIONS 91

APPENDIX B: FABRICATION OF EVAPORATED Au-n TYPE Si CONTACTS 94

APPENDIX C: DATA ANALYSIS COMPUTER PROGRAM 111

REFERENCES 116

LIST OF SYMBOLS

A	Richardson's Constant.
a	The area of the metal contact to the semiconductor.
a	Lattice constant of semiconductor.
b	Variable defined by Eq. 2.42
C_n	Net capture rate for electrons.
C_p	Net capture rate for holes.
C_1, C_2	Integration constants.
c.p.	Cyclic permutation.
c_{11}, c_{12}, c_{44}	Elastic stiffness constants.
D_d	Shift per unit dilation of the band edge.
D_n	The diffusion constant for electrons in the semiconductor.
D_p	The diffusion constant for holes in the semiconductor.
D_u	Half the splitting of the band edge for uniaxial strain along the (100) axis.
$D_{u'}$	Half the splitting of the band edge for uniaxial strain along the band edge.
E	Strain dependent allowed energy.
ΔE	Energy difference in unstrained silicon between the Δ_1 and $\Delta_{2'}$ bands at the band edge.
E_c	Minimum allowed energy of the conduction band.
$E_{c_1}, E_{c_2}, E_{c_3}$	Strain dependent minimum allowed energy of the conduction band along the (100), (010) and (001) directions.

$\Delta E_{c_1}, \Delta E_{c_2}, \Delta E_{c_3}$	Strain dependent shift in the conduction band minimum along the (100), (010) and (001) directions respectively.
E_F	Fermi-energy level.
ΔE_F	Strain dependent shift in the Fermi energy.
E_g	Forbidden energy gap of the semiconductor.
ΔE_g	Stress dependent shift in the forbidden gap.
E_i	Intrinsic energy level of semiconductor.
E_o	Zero strain allowed energy.
$\mathscr{E}_o$	Maximum energy of filled surface states in the semiconductor.
E_t	Energy level of the traps.
E_v	Maximum allowed energy of the valence band.
$\Delta E_{v_1}, \Delta E_{v_2}$	Strain dependent changes in the heavy and light hole $\Gamma_{25}(J = 3/2)$ bands respectively.
e	A general strain
$e_r(r = 1, 2, \ldots, 6)$	Engineering strain.
$e_{\alpha\beta}(\alpha, \beta = x, y, z)$	Conventional strain.
$e_{ij}(i, j = 1, 2, 3)$	Tensor stress.
F_n	Quasi-Fermi energy for electrons.
F_p	Quasi-Fermi energy for holes.
F_t	Quasi-Fermi energy for the traps.
f(b)	Function defined by Eq. 2.41.

f_t	Fraction of traps occupied by electrons.
f_{tp}	The fraction of traps occupied by holes.
G	The generation rate for hole—electron pairs in the semiconductor.
H	Strain dependent Hamiltonian.
H_o	Zero strain Hamiltonian.
h	Planc's Constant.
$\hbar$	Planc's Constant divided by 2π.
I	Current.
I_n	The electron (Schottky) current.
I_{no}	Schottky saturation current.
I_p	Current carried by holes.
I_{p_o}	Minority carrier saturation current.
I_r	Space-charge recombination current.
I_{rs}	Surface recombination current.
J	Angular momentum quantum number.
$J_n, J_n(x)$	The density of current carried by electrons.
$J_p, J_p(x)$	The density of current carried by holes.
J_r	Space-charge recombination current density.
J_{rs}	Surface recombination current density.
J_x, J_y, J_z	x, y and z components of the angular momentum matrices for the holes in the $\Gamma_{25'}$ level.
K_x	(100) component of $\underline{k}$ as measured from X_1.
$K_{x_{min}}$	Strain dependent position of the conduction band minima as measured from X_1.

k	Boltzmann's Constant.
$\underline{k}$	Quantum mechanical wave vector.
k_x, k_y, k_z	Components of the wave vector along the (100), (010) and (001) directions respectively.
m	The mass of an electron.
$m_{c_1}, m_{c_2}, m_{c_3}$	Effective mass of an electron in a conduction band minimum along the (100), (010) and (001) directions respectively.
m_v^*	Mean effective mass of holes in the heavy and light hole $\Gamma_{25'}(J = 3/2)$ band.
m_{v_1}, m_{v_2}	Effective mass of a hole in the heavy and light hole $\Gamma_{25'}(J = 3/2)$ bands respectively.
m_{v_3}	Effective mass of a hole in the split off $\Gamma_{25'}(J = 1/2)$ band.
$m_{\parallel}$	Effective mass of conduction band electrons in silicon as measured along the (100) direction.
$m_{\perp}$	Effective mass of conduction band electrons in silicon as measured perpendicular to the (100) direction.
N	A conduction band parameter.
N_A	The density of acceptor atoms in the semiconductor.
N_D	The donor density in the semiconductor.
N_{ss}	Density of surface states.
$n, n(x)$	The density of conduction band electrons in the semiconductor.
n_i	Density of intrinsic carriers in the semiconductor.
n_o	Zero stress equilibrium electron density.
n_{os}	Equilibrium electron concentration at the interface of a rectifying metal-semiconductor contact.

n_1	Density of conduction band electrons when the Fermi-level falls at the trap energy.
p, p(x)	The density of valence band holes in the semiconductor.
p_n	Density of holes in bulk n-type semiconductors.
p_o	The zero stress equilibrium hole density.
p_{os}	Equilibrium hole concentration at the interface.
p_{no}, n_{po}	Zero strain minority carrier density.
p_1	Density of valence band holes when the Fermi energy falls at the trap energy.
q	The electronic charge.
R_c	Radius of the metal contact.
R_s	Series resistance of the bulk silicon, approximately equal to the spreading resistance.
$\mathscr{R}$	Rate of recombination for nonequilibrium but steady-state conditions.
$\mathscr{R}_s$	Rate of recombination at the surface of the semiconductor.
s_{11}, s_{12}, s_{44}	Elastic compliance constants.
T	The absolute temperature.
U	Applied potential that appears across the space-charge region of a rectifying metal-semiconductor contact.
V(x)	Potential function which describes the band bending of the bottom of the conduction band in the semiconductor.
V	A conduction band parameter.
V_a	Potential applied to the terminals of the rectifying metal-semiconductor contact.

V_D	Diffusion potential of a rectifying metal-semiconductor contact.
v_{no}	Surface recombination velocity for electrons.
v_{po}	Surface recombination velocity for holes.
v_{th}	Thermal velocity of the current carriers.
W	Width of the space-charge region in the semiconductor.
X_1	Conduction band at $\underline{k} = \pi a^{-1}$ (200).
x	The distance measured from the metal-semiconductor interface into the semiconductor.
$y = x - W$	
Z_1, Z_2	Integration limits defined by Eq. 2.43.
α	Proportionality constant.
$\Gamma_{25'}$	Valence band energies.
$\Gamma_{25'}(J = 3/2)$	"Light" and "Heavy" hole band energies.
$\Gamma_{25'}(J = 1/2)$	"Split-Off" valence band energy.
$\gamma(\sigma)$	Ratio of stress dependent minority carrier density to zero strain minority carrier density for highly doped material.
Δ_1, Δ_2	Conduction bands of silicon.
ϵ	The dielectric constant of the semiconductor.
η	Factor used to describe the slope of the linear portion of a foward biased experimental V-I characteristic.
μ_n	The mobility of electrons in the semiconductor.
μ_p	The mobility of holes in the semicondcutor.

Ξ_d, Ξ_u, $\Xi_{u'}$	Deformation potential coefficients for the conduction band.
ρ	Resistivity of the semiconductor.
$\rho(x)$	The space charge in the semiconductor.
$\sum_n$, $\sum_p$	Capture cross sections of the surface states for electrons and holes respectively.
σ	General compressive stress.
$\sigma_r(r = 1, 2, \ldots, 6)$	The engineering components of stress.
$\sigma_{\alpha,\beta}(\alpha, \beta = x, y, z)$	Conventional stress.
$\sigma_{ij}(i, j = 1, 2, 3)$	Tensor stress.
τ_n	The lifetime of electrons in the semiconductor.
τ_p	The lifetime of holes in the semiconductor.
τ_{no}	Lifetime of electrons injected into highly p-type material.
τ_{po}	Lifetime of holes injected into highly n-type material.
φ_B	Electronic barrier as seen by electrons in the metal.
φ_n	Energy difference in the bulk between the minimum allowed energy of the conduction band and the Fermi energy.
ϕ_m	Metallic work function.
ϕ_{sc}	Semiconductor work function.
χ_e	Electron affinity of the semiconductor.

LIST OF TABLES

Table	Title	Page
2.1	Metal Semiconductor Barriers.	10
3.1	Deformation Potential Coefficients (ev/unit dilation) for Si. (Kleinman's theoretical values are shown in brackets.)	38
3.2	Values of the Shear Deformation Potential Coefficient D_u, for Boron Doped Si as a Function of Doping Concentration. [After Wortman[3-10].]	39
3.3	Calculated Change in Energy Levels in ev x σ x 10^{-12} cm^2/dyn of Si for Hydrostatic, Uniaxial [100], Uniaxial [111] and Uniaxial [011] Compression Stresses.	40

LIST OF FIGURES

Figure	Title	Page
2.1	Flat Energy Band Diagram for n-Type Semiconductor.	5
2.2	Energy Band Diagram of Rectifying Contact.	7
2.3	Barrier Height (φ_B) as a Function of Band Gap (E_g) for Various Semiconductors. [After Mead and Spitzer[2-4].]	11
2.4	Energy Band Diagrams Showing Quasi-Fermi Levels for Forward Biased Diodes.	20
3.1	Energy Band Structure of Silicon for the [111] and [100] Directions in $\underline{k}$ Space. [After Philips[3-1].]	30
3.2	Multivalley Constant Energy Surfaces for the Conduction Band Electrons of Si. [After Mason and Bateman[3-2].]	30
3.3	$\Gamma_{25'}$, Energy Level for Si. [After Mason and Bateman[3-2].]	31
3.4	Cross Section of Valence Band Energy Surfaces of Si a Constant Distance Below the Origin. [After Mason and Bateman[3-2].]	31
3.5	Variation of Band Edge Point as Measured for the Origin in the (100) Direction with Respect to Shear Strain e_4. [After Wortman[3-11].]	36
3.6	Ratio of Minority Carrier Density with Stress to the Unstressed Minority Carrier Density $\gamma(\ )$ as a Function of Stress in Si. Values are Given for Hydrostatic, [100], [111], and [001] Uniaxial Compression Stresses. [After Wortman et al.[3-14].]	46

Figure	Title	Page
3.7	One-Dimensional Energy Band Diagrams for Si.	46
3.8	Energy Band Diagram of Metal-Semiconductor Contact.	49
3.9	Schottky Current Volt-Ampere Characteristic with Stress Dependent Barrier Height.	51
3.10	Space-Charge Recombination Current Volt-Ampere Characteristic with Stress Dependent n_i and Constant $E_t - E_i$.	56
3.11	Space-Charge Recombination Current Volt-Ampere Characteristic with Constant n_i and Various Values for $E_t - E_i$.	57
4.1	Photograph of Electrical Test Setup.	64
4.2	Schematic of Electrical Test Setup.	65
4.3	Stylus Points.	67
4.4	Zero Stress Volt-Ampere Characteristic of Typical Planar Gold-Silicon Contact.	69
4.5	Thermal Activation Energy Plot of the Saturation Current.	74
4.6	Zero Stress Volt-Ampere Characteristic of Typical Mesa Gold to n-Type Si Contact.	76
4.7	Volt-Ampere Characteristic of Mechanically Stressed Planar Diode.	80
4.8	Photograph of Stressed Gold Contact (400 X).	81
4.9	Stress Dependent Change in Barrier Height of Planar Diode.	83
4.10	Stress Dependence of Barrier Height (Average of 7 Diodes).	84
4.11	Forward Volt-Ampere Characteristic.	87

Figure	Title	Page
B. 1	Mechanical Polishing Arrangement.	96
B. 2	Rotary Etching Arrangement.	97

CHAPTER I

INTRODUCTION

Studies of the effect of mechanical stress on the volt-ampere characteristic of a rectifying metal-semiconductor contact were undertaken as early as 1929[1-1]. The early explanations[1-2] of the effect considered only the stress dependent area of the point contact and the possibility of piezoelectric or piezoresistance effects. At this time it was impossible to explain the stress effect since there was no theory available which adequately described the rectification process. In 1938[1-3] and 1939[1-4], Schottky showed how rectification could be described on the basis of the formation of a potential energy barrier in the semiconductor. However, as late as 1959[1-5] the stress effect in point contact diodes was still discussed in terms of the stress dependent area changes even though the correlation with experimental results was not satisfactory.

In 1962 Rindner published a number of papers[1-6 to 1-9] which dealt with the effect of mechanical stress on the volt-ampere characteristic of p-n junctions. He explained the phenomenon by postulating that the application of compressive stress introduces a large number of generation-recombination centers into the junction. According to Rindner, these centers disappear when the stress is removed.

This theory was discounted by Wortman et al.[1-10] who developed a model based on the stress dependent shift in the electronic energy bands of the semiconductor. Since Wortman's theory was quite successful in explaining the stress effect in p-n junctions, the author felt that it would now be possible to explain the stress effect in a rectifying metal-semiconductor contact.

The discussion in this report begins with a development of the equations which approximately describe the various current components in a rectifying contact (Chapter II). Then the expected effect of mechanical stress on each component is considered (Chapter III). However, on examination of the experimental data (Chapter IV), it is soon apparent that the effect of mechanical stress on the volt-ampere characteristic of metal-semiconductor contacts is extremely complex.

An extension of Wortman's theory is presented which predicts a stress dependent change in the potential energy barrier height of the contact. Although this is observed, it is almost completely overshadowed by the appearance of large changes in the recombination current components. These changes do not correlate with the band shifting theory of Wortman. The reason (or reasons) for the large changes in the recombination currents is difficult to determine since the origin of these currents is not well understood. In addition, the mathematical expressions for these currents contain various quantities

which are impossible to determine precisely. The author has, therefore, chosen to show the reader what happens to the recombination currents if the numerical values for some of these quantities are changed. Chapter IV includes a discussion of how these numerical changes may correlate with the stress-dependent motion of crystalline defects.

This report on the effect of mechanical stress on rectifying metal-semiconductor contacts begins with the development of equations for the current components which may exist in the device.

CHAPTER II

RECTIFYING METAL-SEMICONDUCTOR CONTACTS

In this chapter the equations which govern the volt-ampere characteristic of a rectifying metal-semiconductor contact are developed on the basis of a simplified potential barrier theory. The current which flows through the contact is assumed to be a summation of four distinct types of current. They are: 1) majority carrier (Schottky) current, 2) minority carrier current, 3) space charge recombination current, and 4) surface recombination current. All modern theories of clean, intimate, rectifying contacts are based on the formation of a potential barrier in the semiconductor. The discussion therefore begins by showing how such a barrier is formed.

2.1 Formation of the Potential Barrier

2.1.1 Potential Barrier for a "Flat-Band" Semiconductor.

The most elementary band theory represents the energy bands of a semiconductor as shown in Fig. 2.1. In this figure the energy bands of the semiconductor are flat from the interior to the surface of the crystal. If a clean metal plate which is in thermodynamic equilibrium with the semiconductor is brought close to the surface of the semiconductor, an electric field appears between the surfaces. The magnitude and direction of the field is determined by the difference

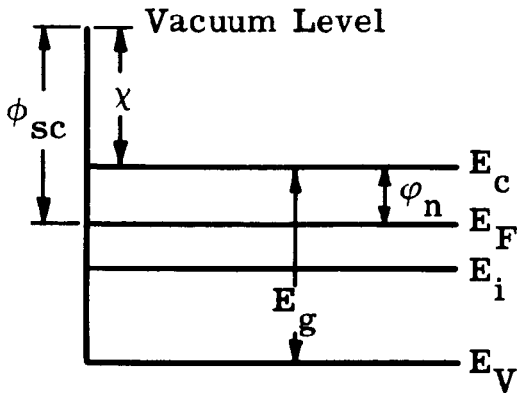


Fig. 2.1 Flat Energy Band Diagram for n-Type Semiconductor

E_c is the minimum allowed energy of the conduction band

E_F is the Fermi energy

E_i is the intrinsic energy

E_V is the maximum allowed energy of the valence band

E_g is the forbidden gap

ϕ_{sc} is the thermionic work function

φ_n is the energy difference, $E_c - E_F$, in the bulk

of the thermionic work functions of the two materials divided by the distance separating them. This electric field induces charge at the surfaces. At the surface of the semiconductor this produces an accumulation or depletion of majority carriers (depending on the direction of the electric field and the conductivity type of the semiconductor). A depletion of majority carriers from the surface of a semiconductor results in a space charge due to a volume distribution of ionized impurity atoms. For example, if a metal whose work function, ϕ_m, is brought into contact with an n-type semiconductor whose work function, ϕ_{sc}, is less than ϕ_m, the energy band diagram shown in Fig. 2.2 results. The + signs in the diagram represent the ionized donor atoms.

It appears from Fig. 2.2 that the barrier height and diffusion potential are predictable on the basis of the relative work functions and the electron affinity. However, this is not the case. The barrier height and diffusion potential of experimental contacts do not depend on the relative work functions. The lack of this dependence was not understood until 1947 when Bardeen[2-1] showed that the potential barrier in the semiconductor is controlled by the surface states of the semiconductor rather than the difference of the thermionic work functions.

2.1.2 Potential Barriers in Semiconductors with Surface States. On a purely theoretical basis, Tamm[2-2] and Shockley[2-3]

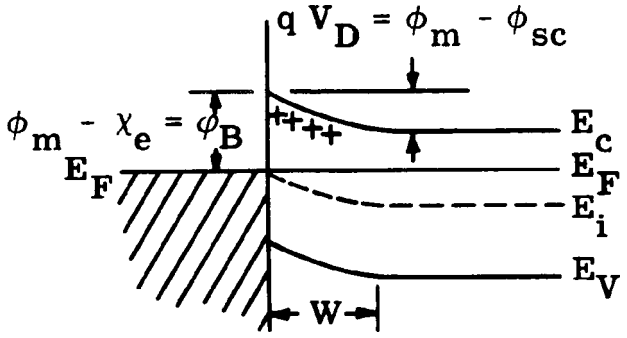


Fig. 2.2 Energy Band Diagram of Rectifying Contact

φ_B is the barrier height

V_D is the diffusion potential

W is the width of the space charge region

showed how the termination of the periodic potential of a crystal can give rise to additional allowed energy levels at the surface (surface states). These surface states may have energy levels which lie in the normally forbidden band. Bardeen[2-1] proposed that electrons from the bulk can be trapped in the surface states, leaving behind an equal and opposite space charge. Thus, a potential barrier is formed near the surface of the semiconductor even in the absence of an adjacent metal contact.

In order to see how charge in surface states affects the formation of a potential barrier at a metal-semiconductor interface, consider the following. Assume that the surface states lying in the forbidden band are filled to some energy, $\mathscr{E}_0$. This is the location of the Fermi energy at the surface when the surface is charge neutral. If an electric field is applied to the surface, charge will be induced on the semiconductor surface. If the surface-state density is high, most of the charge will be induced in the surface states and the Fermi level shifts from $\mathscr{E}_0$. However, the shift in the Fermi level will be much smaller than it would be if no surface states were present. Therefore, in the case of a metal-semiconductor contact, the barrier height will not be a strong function of relative work functions if surface states are present.

For some semiconductors the surface-state density is so large that the barrier height is insensitive to the type of metal used to make

the contact.[2-4, 2-5] See Table 2. 1. For those semiconductors with approximately constant barrier height, the barrier height is on the order of $\frac{2}{3} E_g$. See Fig. 2. 3.

Regardless of the details of the formation process, a barrier-type of contact between a metal and an n-type semiconductor can be represented as shown in Fig. 2. 2 when φ_B or V_D are determined experimentally.

2. 1. 3 Functional Form of the Band Bending. The variation of the band extrema with position can be found by defining a potential function, V(x), such that qV(x) is the potential energy of an electron at the bottom of the conduction band. If the position of the Fermi level in the metal is taken as reference, V(x), which describes the bending of the conduction band minimum, can be found from Eq. 2. 1.

$$\nabla^2 V(x) = \frac{-\rho(x)}{\epsilon} = \frac{-q}{\epsilon} [N_D - n(x) - N_A + p(x)] \qquad (2.1)$$

where N_D is the density of ionized donor atoms, N_A is the density of ionized acceptor atoms, n(x) is the density of electrons in the conduction band, p(x) is the density of holes in the valence band, ϵ is the dielectric constant of the semiconductor, and q is the electronic charge. The boundry conditions for the equation are

$$V(0) = -V_D - \frac{\varphi_n}{q}$$

and (2. 2)

$$V(\infty) = -\frac{\varphi_n}{q} - U$$

Table 2. 1

Metal Semiconductor Barriers

Reference	Semiconductor (Surface Prep)	Energy Gap (ev)	Metal	Barrier Height (ev)*		
				V-I	Cap**	Photo
2-4 2-4	n AlAs (Vac Cleave)	2. 4	Au Pt			1. 2 1. 0
2-4	p AlSb (Vac Cleave)	1. 5	Au		0. 53	0. 55
2-4	p BN (Chem)	9. 8	Au		3. 1	
2-6	p BP	6. 1	Au			0. 87
2-4	p C [Diamond]	5. 6	Au		1. 35	
2-4	n GaAs (Vac Cleave)	1. 4	Au Pt Be Ag Cu Al		0. 95 0. 94 0. 82 0. 93 0. 87 0. 80	0. 90 0. 86 0. 81 0. 88 0. 82 0. 80
2-4	p GaAs (Vac Cleave)	1. 4	Au Au (77°) Pt (77°) Ag (77°) Cu (77°) Al Al (77°)		0. 48 0. 46 0. 48 0. 44 0. 52 0. 63 0. 61	0. 42 0. 50
2-7	n Ga P	2. 24	Au	1. 1	1. 3	1. 3
2-8	n Ga P (Chem)		Cu Al Au Pt Mg Ag		1. 34 1. 14 1. 34 1. 52 1. 09	1. 20 1. 05 1. 28 1. 45 1. 04 1. 2
2-4	n Ge (Vac Cleave) n Ge	0. 68	Au W	 0. 48	0. 45	
2-4	n InSb	0. 18	Au (77°) Ag (77°)		0. 17 0. 18	
2-10	n Pb O	2. 3	Ag Bi Ni Pb In			0. 95 0. 94 0. 96 0. 95 0. 93
2-11	n Si (Vac Cleave)	1. 1	Al Ag Cu Ni Pd Pt Au		0. 25 0. 39 0. 40 0. 5 0. 58 0. 76 0. 78	
2-4	SiC (Chem) (Hex)	2. 9	Au Al		1. 95 2. 0	

*The value of the barrier height in a metal-semiconductor contact can be determined by three different techniques: 1) from the volt-ampere characteristic, 2) from the variation of the differential capacitance as a function of bias potential, 3) from the frequency dependence of a photocurrent. The barriers are measured from valence band edge on p-type samples and from the conduction band edge on n-type samples.

**These values are corrected for the position of the Fermi level.

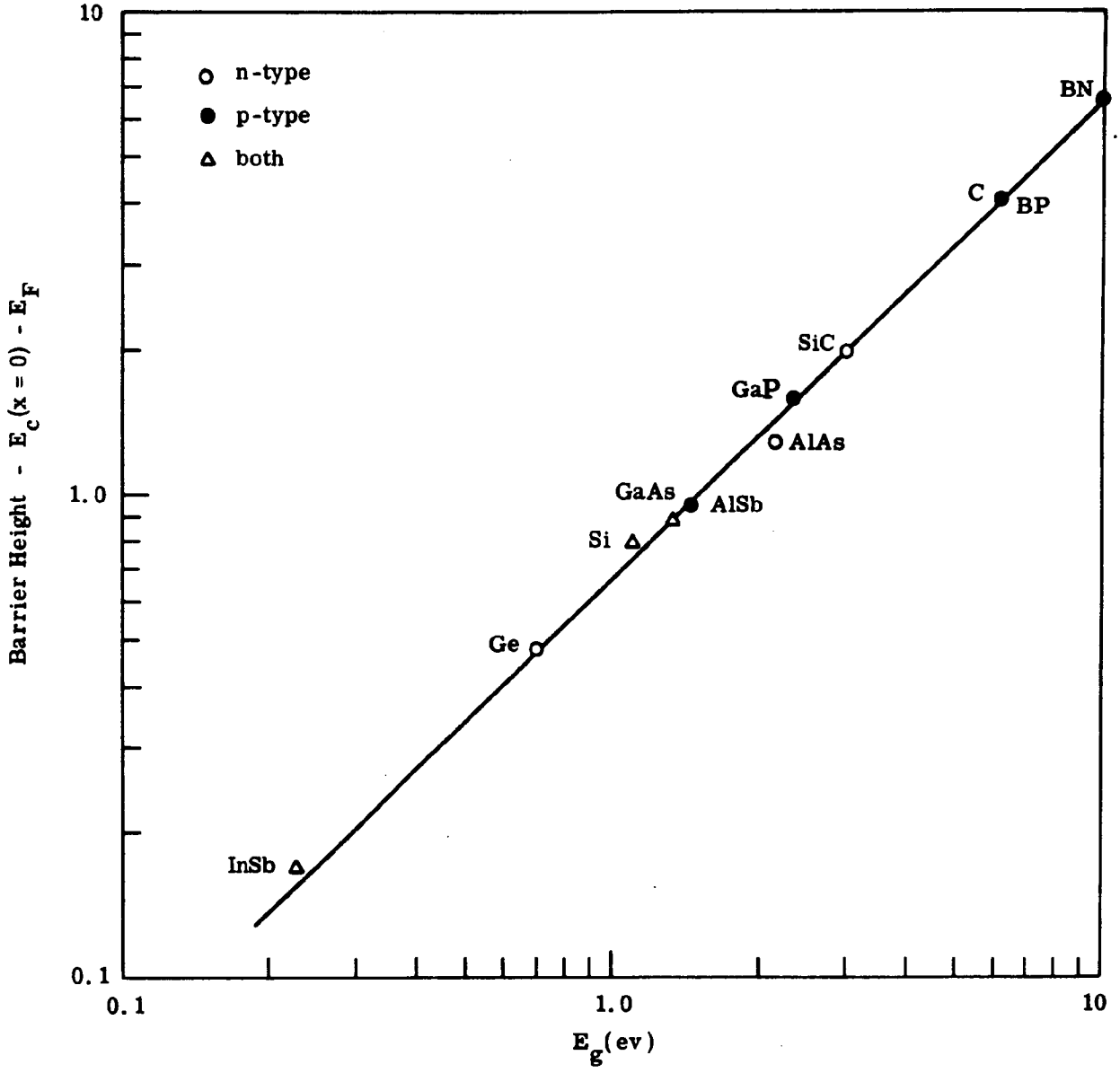


Fig. 2.3 Barrier Height (φ_B) as a Function of Band Gap (E_g) for Various Semiconductors. [After Mead and Spitzer[2-4].]

where U is the potential applied to the contact ($U > 0$ for forward bias and $U < 0$ for reverse bias).

The problem that arises in this technique is that of determining the space charge distribution. The potential variation in the space charge region and the distribution of the carrier densities are interrelated through the transport equations and the continuity equations. For d.c. steady state the continuity equations are

$$0 = G - \frac{n(x) - n_o}{\tau_n} + \frac{1}{q} \nabla \cdot J_n(x) \tag{2.3}$$

and

$$0 = G - \frac{p(x) - p_o}{\tau_p} - \frac{1}{q} \nabla \cdot J_p(x) \tag{2.4}$$

where G is the rate of generation of hole-electron pairs per unit volume, n_o and p_o are the equilibrium distributions of the carrier densities, τ_n and τ_p are the carrier lifetimes, and J_n and J_p are the current densities. The current densities are found from the transport equations

$$J_n = -q \mu_n n(x) \nabla V(x) + q D_n \nabla n(x) \tag{2.5}$$

$$J_p = -q \mu_p p(x) \nabla V(x) - q D_p \nabla p(x) \tag{2.6}$$

where the μ's are the carrier mobilities and the D's are the diffusion coefficients.

For an exact solution, the continuity equations, the transport equations and Poisson's equation must be solved simultaneously. In general this cannot be done analytically without making some judicious approximations. For the purpose of this discussion the potential variation in the barrier is not as important as the height of the barrier.

However, the barrier width, W, appears as a factor in the expression for the space charge recombination current (see Eq. 2.40). Later, in Chapter III, when the effect of stress is considered, it will be necessary to know how W depends on the various other parameters of the contact. In order to get an "order of magnitude" measure of the barrier width, a uniform space charge can be assumed.

$$\left.\begin{aligned} \rho(x) &= N_D \qquad \text{for} \qquad 0 < x < W \\ \rho(x) &= 0 \qquad \text{for} \qquad x > W \end{aligned}\right\} \tag{2.7}$$

Poisson's equation can then be solved directly without using the continuity and transport equations. With the boundry conditions

$$\left.\begin{aligned} V(0) &= -V_D - \frac{\varphi_n}{q} \\ V(W) &= -\frac{\varphi_n}{q} - U \\ \left.\frac{dV}{dx}\right|_{x=W} &= 0 \end{aligned}\right\} \tag{2.8}$$

the solution to Poisson's equation is

$$V(x) = \frac{-q N_D}{2\epsilon} x^2 + \frac{q N_D W}{\epsilon} x - V_D + \frac{\varphi_n}{q} \qquad (0 \leq x \leq W) \qquad (2.9)$$

where

$$W = \sqrt{\frac{2\epsilon}{q N_D} (V_D - U)} \qquad (2\text{-}10)$$

Note that the potential rise, V_D, is assumed to be greater than $\frac{kT}{q}$. Thus, the potential rise acts as a barrier to the flow of electrons. In addition, W is assumed to be much greater than the wavelength of the electrons in the conduction band. Therefore, there is no significant tunnelling current through the barrier.

2.2 Majority Carrier (Schottky) Current

In this section only the current carried by electrons which pass over the potential barrier is considered. There are two components of this current. 1) A current flow of electrons from the metal over the barrier, φ_B, into the semiconductor; and 2) a current flow of electrons from the semiconductor over the barrier, $q(V_D - U)$, into the metal.

An expression for the first current component is found by considering the metal to be a thermionic emitter of electrons which have a Fermi-Dirac energy distribution. The resulting current is[2-12]

$$I = -a\left[\frac{4\pi\, qm\, k^2}{h^3}\right] T^2 \exp\left(\frac{-\varphi_B}{kT}\right) \qquad (2.11)$$

where a is the area of the contact, m is the mass of the electrons, k is Boltzmann's constant, h is Planck's constant, and T is the absolute temperature. Conventional current flow from the metal into the semiconductor is taken to be a positive (forward) current. Equation 2. 11 can be written as

$$I = -a A T^2 \exp\left(\frac{-\varphi_B}{kT}\right) , \qquad (2.12)$$

where A is Richardson's constant and has a theoretical value of 120 amp/cm^2.

An expression for the second current component is similarly found by considering the semiconductor to be a thermionic emitter of electrons which have a Maxwell-Boltzman energy distribution. In this case the barrier that the electrons must surmount is dependent upon the applied voltage. The resulting current is[2-13]

$$I = a q N_D \left(\frac{kT}{2\pi m}\right)^{1/2} \exp\left(\frac{-q}{kT}(V_D - U)\right) . \qquad (2.13)$$

Therefore, the net majority carrier current across the contact is

$$I = \left[a q N_D \left(\frac{kT}{2\pi m}\right)^{1/2} \exp\left(\frac{-q V_D}{kT}\right)\right] \exp\left(\frac{qU}{kT}\right) - \left[a A T^2 \exp\left(\frac{-\varphi_B}{kT}\right)\right] \qquad (2.14)$$

When the potential, U, applied to the contact is zero, there must be no net current. Thus, the quantities in the square brackets in the above equation are equal and the equation can be rewritten as

$$I = a\,AT^2 \exp\left(\frac{-\varphi_B}{kT}\right) \left[\exp\left(\frac{qU}{kT}\right) - 1\right] \quad . \tag{2.15}$$

If the volt-ampere characteristic of an experimental diode is described by the above equation, the diode is commonly referred to as a Schottky Barrier diode and the current as a Schottky current.

2.3 Minority Carrier Current

An approximate expression for the minority carrier current (hole current in this discussion) is derived by analogy to the minority carrier current in a p-n junction.

The continuity and transport equations for the region $x > W$ can now be considered. For convenience define a new variable:

$$y \triangleq x - W \quad . \tag{2.16}$$

For d.c. steady state the continuity equation for holes is

$$O = \frac{p(y) - p_n}{\tau_p} - \frac{1}{q} \nabla \cdot J_p \tag{2.17}$$

where p_n is the equilibrium hole concentration. The transport equation is

$$J_p = -q\,D_p \nabla\, p(y) \tag{2.18}$$

where the drift term is neglected since potential variations for $y > 0$ are small. Combining these two equations yield a second-order differential equation for p(y).

$$\nabla^2 p(y) - \frac{p(y) - p_n}{\tau_p} = 0 \quad . \tag{2.19}$$

The general solution is

$$p(y) = p_n + C_1 \exp \frac{y}{\sqrt{\tau_p D_p}} + C_2 \exp \frac{-y}{\sqrt{\tau_p D_p}} \quad . \tag{2.20}$$

Since p(y) cannot increase indefinitely with y, C_1 must be zero. C_2 can be evaluated by consideration of the hole density at $y = 0$. Using the Boltzman factor, consider the density of holes at the interface which have sufficient energy to diffuse "under" the barrier, $q(V_D - U)$.

$$p(y=0) = p(x=0) \exp\left(\frac{-q(V_D - U)}{kT}\right) . \tag{2.21}$$

Therefore,

$$p(y=0) = p_n \exp\left(\frac{qU}{kT}\right) . \tag{2.22}$$

The minority carrier current density can now be found from Eq. 2.17

$$J_p = q\sqrt{\frac{D_p}{\tau_p}}\, p_n \left[\exp\left(\frac{qU}{kT}\right) - 1\right] \exp\left(\frac{W - x}{\sqrt{\tau_p D_p}}\right) \quad . \tag{2.23}$$

Thus, the minority carrier injection current is

$$I_p = a\, q\, p_n \sqrt{\frac{D_p}{\tau_p}} \left[\exp\left(\frac{qU}{kT}\right) - 1\right] \quad . \tag{2.24}$$

2.4 Space Charge Recombination Current

The space charge recombination current for a rectifying-metal-semiconductor contact is also developed by analogy to the case for the p-n junction. This development uses the recombination statistics of Schockley, Read, and Hall[2-14, 2-15, 2-16] and follows the analysis of Sah et al.[2-17]

In the d.c. steady state case it is possible to maintain a non-equilibrium carrier density in the space charge region of the semiconductor. For this situation it is convenient to define "quasi-Fermi" levels such that the carrier densities can be found from a Boltzman relation, i.e.,

$$n = n_i \exp\left(\frac{F_n - E_i}{kT}\right) \tag{2.25}$$

and

$$p = n_i \exp\left(\frac{E_i - F_p}{kT}\right) \tag{2.26}$$

where F_n and F_p are the quasi-Fermi levels for electrons and holes, respectively. Thus, the p-n product is

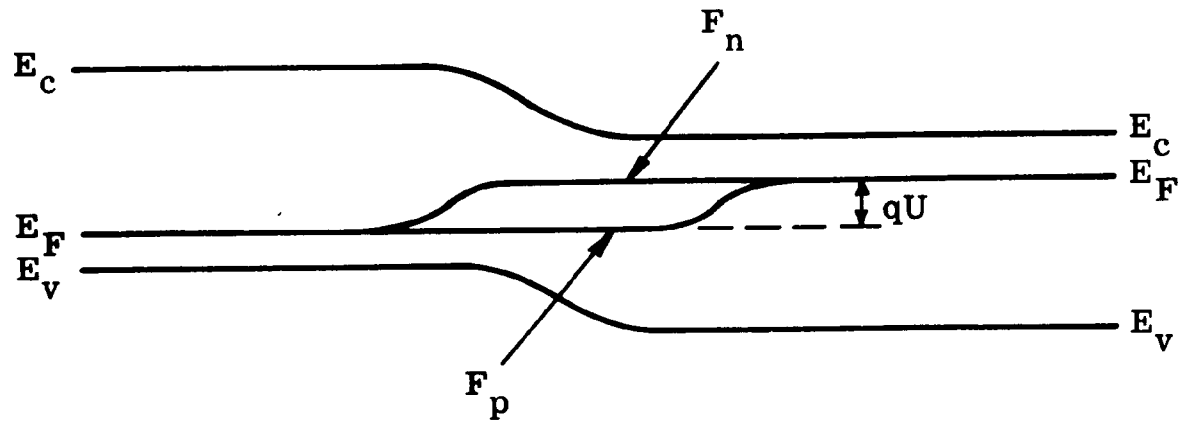
$$pn = n_i^2 \exp\left(\frac{F_n - F_p}{kT}\right) \quad . \tag{2.27}$$

For the case of a p-n junction with forward bias applied, the quasi-Fermi levels are assumed to be flat through the charge depletion region as shown in Fig. 2.4(a). Figure 2.4(b) shows the analogous assumption for the case of a metal-semiconductor contact. As shown in the figure, the separation of the quasi-Fermi levels is just the potential, U. With this assumption the p-n product is

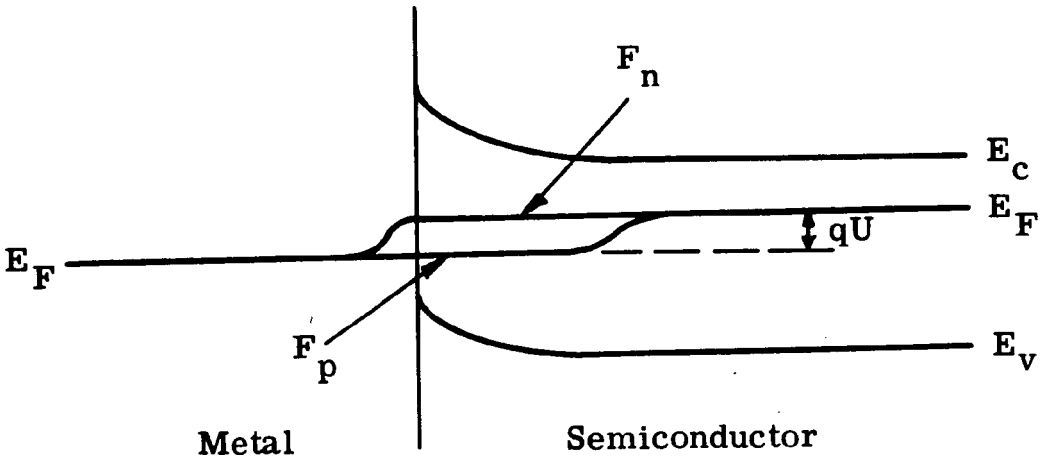
$$pn = n_i^2 \exp\left(\frac{qU}{kT}\right) \quad . \tag{2.28}$$

Assume now that there are generation-recombination centers uniformly distributed in the semiconductor. Assume also that these centers of traps have a single energy level, E_t, in the forbidden band. There are two processes by which recombination may take place. 1) If the trap is occupied by a hole, an electron may drop into the trap and recombine with the hole. 2) If the trap is occupied by an electron, a hole may jump from the valence band into the trap and recombine with the electron. There are also two processes by which carriers may be generated. 1) If the trap is occupied by an electron, it may emit that electron into the conduction band. 2) If the trap is occupied by a hole, it may emit that hole into the valence band.

The rate of capture of conduction band electrons by the traps can be expressed as



(a) Forward Biased p-n Junction



(b) Forward Biased Metal-Semiconductor Contact

Fig. 2.4 Energy Band Diagrams Showing Quasi-Fermi Levels for Forward Biased Diodes

$$\frac{n f_{tp}}{\tau_{no}} \tag{2.29}$$

where n is the density of conduction band electrons, τ_{no} is the lifetime for electrons injected into highly p-type material, and f_{tp} is the fraction of traps occupied by holes. The rate that electrons are generated from traps into the conduction band can be expressed as

$$\alpha f_t \tag{2.30}$$

where f_t is the fraction of traps occupied by electrons and α is a proportionality constant which includes the trap density, the total number of empty electronic states in the conduction band and the probability per unit time of an electron emission from the trap. Note that

$$f_t = 1 - f_{tp} \quad . \tag{2.31}$$

It is convenient to introduce a quasi-Fermi level, F_t, for the traps. The fraction of traps occupied by electrons can then be expressed as

$$f_t = \frac{1}{1 + \exp\left(\frac{E_t - F_t}{kT}\right)} \quad . \tag{2.32}$$

For the case of thermal equilibrium, the rate of capture of electrons must equal the rate of emission. Equating these two rates, the proportionality constant, α, is determined.

$$\alpha = \frac{n_i}{\tau_{no}} \exp\left(\frac{E_t - E_i}{kT}\right) = \frac{n_1}{\tau_{no}} \tag{2.33}$$

where n_1 is the density of conduction band electrons when the Fermi level falls at E_t. The net capture rate for electrons in a nonequilibrium situation is

$$C_n = \frac{(n\, f_{tp} - n_1\, f_t)}{\tau_{no}} \quad . \tag{2.34}$$

Similarly, the net capture rate for holes in a nonequilibrium situation is

$$C_p = \frac{(p\, f_t - p_1\, f_{tp})}{\tau_{po}} \tag{2.35}$$

where τ_{po} is the lifetime of holes injected into highly n-type material and p_1 is

$$p_1 = n_i \exp\left(\frac{E_i - E_t}{kT}\right) \quad . \tag{2.36}$$

The rate of recombination for nonequilibrium but steady state conditions, $\mathscr{R}$, is found by requiring that the rate of electron capture be equal to the rate of hole capture

$$\mathscr{R} = C_n = C_p \quad . \tag{2.37}$$

This leads to

$$f_t = \frac{n\,\tau_{po} + p_1\,\tau_{no}}{(n + n_1)\,\tau_{po} + (p + p_1)\,\tau_{no}} \tag{2.38}$$

which makes the steady state recombination of carriers

$$\mathscr{R} = \frac{pn - n_i^2}{(n + n_1)\,\tau_{po} + (p + p_1)\,\tau_{no}} \tag{2.39}$$

The current density resulting from recombination in the space charge region is

$$J_r = q \int_0^W \mathscr{R}\, dx \tag{2.40}$$

For the case of small applied potential, Sah et al.[2-17] show that with a linear approximation to the potential variation, the integration can be performed. The result is

$$J_r = \frac{q\,n_i}{\sqrt{\tau_{no}\,\tau_{po}}}\, W\, \frac{2 \sinh\left(\frac{qU}{2kT}\right)}{\frac{(V_D - U)}{kT}}\, f(b) \tag{2.41}$$

where

$$f(b) = \int_{Z_1}^{Z_2} \frac{dZ}{Z^2 + 2\,bZ + 1} \quad , \tag{2.42}$$

$$b = \exp\left(\frac{-qU}{2kT}\right) \cosh\left\{\frac{E_t - E_i}{kT} + \frac{1}{2}\,\ell n\,\frac{\tau_{po}}{\tau_{no}}\right\} \quad ; \tag{2.43}$$

and

$$Z_1, Z_2 = \sqrt{\frac{\tau_{po}}{\tau_{no}}} \exp\left(\frac{\mp q(V_D - U)}{kT}\right) \quad . \tag{2.44}$$

This expression for the space charge recombination current is a bit too complex to be useful in interpretating experimental diode characteristics. Hauser[2-18] has developed an approximate expression for Sah's result.

$$J_r = \frac{q\, n_i^2\, W\left[\exp\left(\frac{qU}{kT}\right) - 1\right]}{(\tau_{po}\, n_1 + \tau_{no}\, p_1) + (\tau_{po} + \tau_{no})\, n_i \exp\left(\frac{qU}{2kT}\right)} \quad . \tag{2.45}$$

This expression has a maximum deviation from Eq. 2.41 for $\tau_{no} = \tau_{po}$ and $n_1 = p_1 = n_i$; however, the maximum deviation is less than an order of magnitude over the whole voltage range.

For the purpose of this study, Hauser's expression for the space charge recombination current is sufficiently accurate. Also, the effect of mechanical stress (Chapter III) on this current can be shown in a more straightforward manner.

The above expression was derived with a p-n junction in mind. However, since it is only the junction region that is specifically involved, this development and the resultant current expressions are appropriate for the space charge region of a metal-semiconductor contact.

2. 5 Surface Recombination Current

Recombination can also take place at the surface states. Just as a lifetime is associated with a bulk recombination center, a "recombination velocity" can be associated with a surface state recombination center. The surface recombination velocity for electrons, v_{no}, and for holes, v_{po}, depends on the density of the recombination centers, the capture cross sections for electrons and holes, respectively, and the thermal velocity of the carriers.

By analogy with the previous section the rate of recombination of carriers at the surface can be written as

$$\mathcal{R}_s = \frac{pn - n_i^2}{(n + n_1)\frac{1}{v_{po}} + (p + p_1)\frac{1}{v_{no}}} \quad . \tag{2.46}$$

Again with the assumption of flat quasi-Fermi levels (see Fig. 2. 4b),

$$\begin{aligned} n &= n_{os} \exp\left(\frac{qU}{kT}\right) \\ p &= p_{os} = \text{const} \end{aligned} \tag{2.47}$$

where n_{os} and p_{os} are the equilibrium carrier concentrations at the interface. The surface recombination current density is therefore,

$$J_{rs} = \frac{q\, n_i^2 \left[\exp\left(\frac{qU}{kT}\right) - 1\right]}{\frac{n_1}{v_{po}} + \frac{p_{so} + p_1}{v_{no}} + \frac{n_i}{v_{po}} \exp\left(\frac{qU}{kT}\right)} \quad . \tag{2.48}$$

Note that for high forward bias, this current density saturates to the value

$$(J_{rs})_{max} = q\, n_i\, v_{po} \quad . \tag{2.49}$$

2.6 Summary

In this chapter the formation of a potential barrier in the semiconductor at the interface of a metal-semiconductor contact is discussed. Typically the barrier height as seen by electrons in the metal (φ_B) or as seen by electrons in the semiconductor ($q\, V_D$) must be determined experimentally. The current which flows through the contact when an external potential is applied is assumed to be composed of four components: (1) A majority carrier (Schottky) current, (2) A minority carrier current, (3) A space charge recombination current, and (4) A surface recombination current. Expressions for each of these currents are listed below for quick reference.

1) Majority carrier (Schottky) current:

$$I_n = a\, A\, T^2 \exp\left(\frac{-\varphi_B}{kT}\right)\left[\exp\left(\frac{qU}{kT}\right) - 1\right] \tag{2.15}$$

2) Minority carrier current:

$$I_p = a\, q\, p_n \sqrt{\frac{D_p}{\tau_p}}\left[\exp\left(\frac{qU}{kT}\right) - 1\right] \tag{2.24}$$

3) Space charge recombination current:

$$I_r = \frac{a\, q\, n_i^2\, W \left[\exp\left(\frac{qU}{kT}\right) - 1\right]}{(\tau_{po}\, n_1 + \tau_{no}\, p_1) + (\tau_{po} + \tau_{no})\, n_i \exp\left(\frac{qU}{2kT}\right)} \qquad (2.45)$$

4) Surface recombination current:

$$I_{rs} = \frac{a\, q\, n_i^2 \left[\exp\left(\frac{qU}{kT}\right) - 1\right]}{\frac{n_1}{v_{po}} + \frac{p_{so} + p_1}{v_{no}} + \frac{n_i}{v_{po}} \exp\left(\frac{qU}{kT}\right)} \qquad (2.48)$$

CHAPTER III

EFFECT OF MECHANICAL STRESS ON THE VOLT-AMPERE CHARACTERISTIC

In this chapter the effect of mechanical stress on the volt-ampere characteristic of a metal-semiconductor contact is developed primarily on the basis of changes which are expected to occur in the semiconductor. A specific semiconductor (silicon) is used as an example of how to account for the effect of stress in the bulk semiconductor. The changes in the bulk are extrapolated to the interface and the stress dependence of the barrier height is determined.

The stress induced changes in the bulk semiconductor and in the barrier height of the contact as well as a speculation of the changes in trap energies are used to calculate the effect of stress on each of the four current components listed in the previous chapter.

3.1 Effect of Stress on the Energy Band Diagram of a Rectifying Contact

The discussion of this section deals solely with metal-silicon contacts. (This is the experimental configuration presented in Chapter IV.) A similar analysis can be performed with other semiconductors provided the strain dependent Hamiltonian and values for the deformation potential coefficients are known.

3.1.1 Stress Dependent Energy Band Diagram for Bulk Silicon. Up to this point in the discussion, a simple band diagram of electron energy verses spatial position has been sufficient. Now, in order to consider the effect of stress, the energy band diagram in momentum space ($\underline{k}$-space) must be used. Figure 3.1 shows the zero-stress energy versus $\underline{k}$-space position diagram for silicon. The shaded area represents the forbidden band. The minimum allowed energy of the conduction band occurs in the (100) directions and are at $\underline{k} = 1.7^{-1}$ (100). Thus the conduction electrons of silicon lie in the six conduction band minima in the (100) directions. As shown in Fig. 3.2, the constant energy surfaces for the electrons in the conduction band are ellipsoids of revolution about the band edge point.

The valence band maximum occurs at $\underline{k}$ = (000). The energy of this maximum is taken as zero. The $\Gamma_{25'}$ energy is shown in an expanded view in Fig. 3.3. This energy level is split into three bands. The lowest band is for electrons with the angular momentum quantum number J = 1/2. The upper two bands are for electrons with the angular momentum quantum number J = 3/2. The splitting of the $\Gamma_{25'}$ (J = 3/2) level is due to spin orbit coupling. The different curvature of the J = 3/2 levels implies different effective masses for electrons at $\underline{k}$ = (000). The upper $\Gamma_{25'}$ (J = 3/2) level contains the

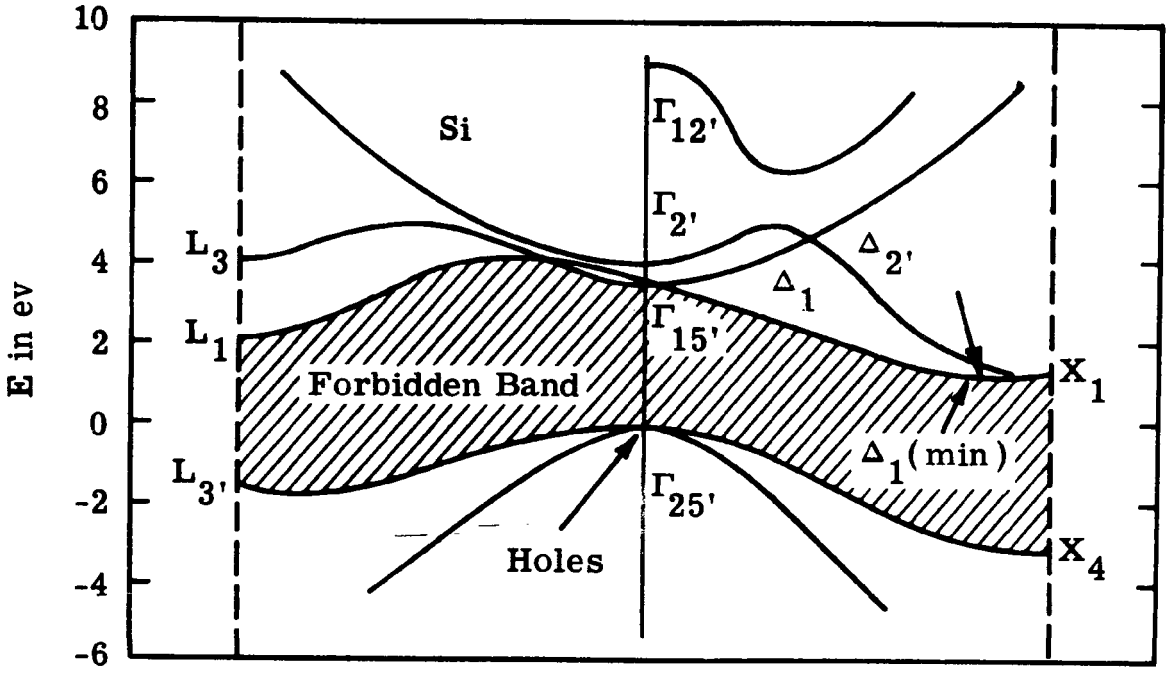


Fig. 3.1 Energy Band Structure of Silicon for the [111] and [100] Directions in $\underline{k}$ Space. [After Philips[3-1].]

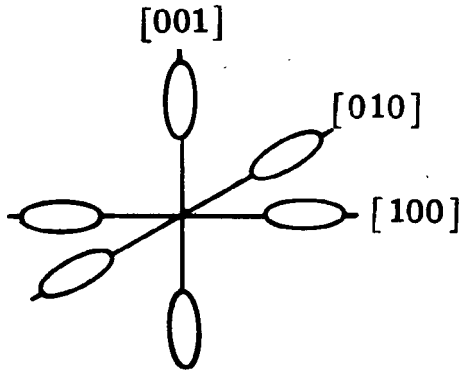
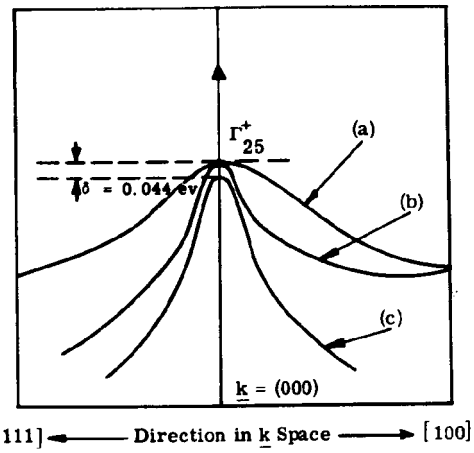


Fig. 3.2 Multivalley Constant Energy Surfaces for the Conduction Band Electrons of Si. [After Mason and Bateman[3-2].]



(a) "Heavy Hole" Band (J = 3/2)

(b) "Light Hole" Band (J = 3/2)

(c) Split-Off Band (J = 1/2)

Fig. 3.3 Γ_{25}, Energy Level for Si.
[After Mason and Bateman[3-2].]

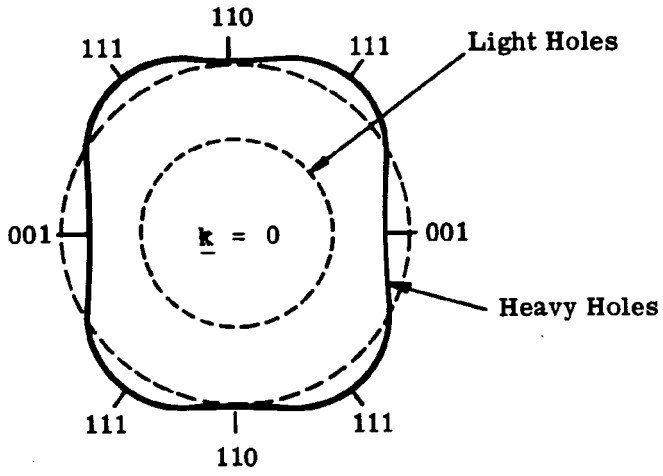


Fig. 3.4 Cross Section of Valence Band Energy Surfaces of Si a Constant Distance Below the Origin.
[After Mason and Bateman[3-2].]

"heavy holes" and the lower $\Gamma_{25'}$ ($J = 3/2$) level contains the "light holes" (see Fig. 3.4).

When the silicon crystal is subjected to a uniaxial stress less than the yield stress, an elastic strain results which produces a change in the lattice periodicity. Because of the dependence of energy levels on lattice spacing, a change in the lattice constant of a crystal implies a change in the electronic structure. A considerable amount of information is available concerning the effect of strain on the electronic band structure of silicon.[3-3 to 3-9] A compilation of this work is presented in a Ph.D. thesis by Wortman.[3-10] The general approach used to find the effect of strain is to consider a band edge, write the strain dependent Hamiltonian for that point and then find the eigenvalues of the Hamiltonian (i.e., the allowed energy levels).

The valence band. For the valence band of a group IV semiconductor, Kleiner and Roth[3-6] write the strain dependent Hamiltonian as

$$H = H_o + D_d(e_1 + e_2 + e_3) + \frac{2}{3} D_u \left[\left(J_x^2 - \frac{1}{3} J^2 \right) e_1 + \text{c.p.} \right] + \frac{2}{3} D_{u'} \left[\frac{1}{2} \left(J_y J_z + J_z J_y \right) e_4 + \text{c.p.} \right] . \quad (3.1)$$

H_o is the zero strain Hamiltonian. The e's are the six strain components (these are defined in Appendix A). The J's are the angular momentum matrices for a hole in the $\Gamma_{25'}$ level. D_d is the shift per

unit dilation of the band edge. $2D_u$ is the splitting of the band edge caused by uniaxial shear strain along the (100) axis. Similarly $2D_{u'}$ is the splitting for the (111) axis. c.p. means cyclic permutations of the x, y, z directions referred to the crystallographic axes. Diagonalizing H, the allowed energy for the $\Gamma_{25'}$, (J = 3/2) level is

$$E = E_o + D_d(e_1 + e_2 + e_3) \pm \left[\left(\frac{2}{3} D_u\right)^2 (e_1^2 + e_2^2 + e_3^2 - e_1e_2 - e_1e_3 - e_2e_3) + \left(\frac{2}{3} D_{u'}\right)^2 (e_4^2 + e_5^2 + e_6^2)\right]^{1/2} , \qquad (3.2)$$

where E_o is the unstrained allowed energy. If the strain is compressional, the + sign corresponds to the heavy hole band and the - sign to the light hole band. If the strain is tensional, the correspondence is reversed. The effect of strain on the $\Gamma_{25'}$, (J = 3/2) level not only shifts the energy level but also removes the degeneracy at $\underline{k}$ = (000).

The same manipulation can be performed for the $\Gamma_{25'}$, (J = 1/2) level. The strain dependent allowed energy for this level is

$$E = E_o + D_d(e_1 + e_2 + e_3) \ . \qquad (3.3)$$

The conduction band. The analysis of the effect of strain on the conduction band of Si is complicated by the fact that the energy minimum is not located at the high symmetry point, X_1. (See Fig. 3.1.) Hensel and Hasegawa[3-6] have shown how the energy minimum shifts in magnitude and $\underline{k}$-space position when the crystal is strained. The strain dependent Hamiltonian is

$$H = \begin{cases} \hbar V K_x + \frac{\hbar^2}{2m_{\parallel}} K_x^2 + \frac{\hbar^2}{2m_{\perp}} (k_y^2 + k_z^2) & \Xi_{u'} e_4 + \hbar^2 N k_y k_z \\ \quad + \Xi_d (e_1 + e_2 + e_3) + \Xi_u e_1 & \\ & -\hbar V K_x + \frac{\hbar^2}{2m_{\parallel}} K_x^2 + \frac{\hbar^2}{2m_{\perp}} (k_y^2 + k_y^2) \\ \Xi_{u'} e_4 + \hbar^2 N k_y k_z & \quad + \Xi_d (e_1 + e_2 + e_3) + \Xi_u e_1 \end{cases} \tag{3.4}$$

where $m_{\parallel}$ and $m_{\perp}$ are the effective masses along the (100) directions and perpendicular to these directions respectively. V and N are band parameters and K_x is the (100) component of the wave vector, $\underline{k}$, as measured from the high symmetry point, X_1.

$$K_x = 2\pi a^{-1} - k_x \ . \tag{3.5}$$

Ξ_d and Ξ_u are the deformation potential coefficients as defined by Herring.[3-4] $\Xi_{u'}$ is introduced by Hensel and Hasegawa[3-6] from symmetry considerations. Diagonalizing the Hamiltonian and setting k_y and k_z equal to zero, the allowed energy bands are given by

$$E = \frac{\hbar^2}{2m_{\parallel}} K_x^2 + \Xi_d (e_1 + e_2 + e_3) \pm \pm \left[\hbar^2 V^2 K_x^2 + \left(\Xi_{u'} e_4 \right)^2 \right]^{1/2} . \tag{3.6}$$

The + sign corresponds to the $\Delta_{2'}$ band and the - sign to the Δ_1 band. Note that the parameter, N, does not appear in this expression.

The value of the parameter, V, can be found by estimating the difference in energy, ΔE, between the Δ_1 and Δ_2, band at the unstrained band edge. Then

$$\Delta E = 2m_{\parallel} V^2 \quad . \tag{3.7}$$

Now if the position of the minimum can be found, the allowed energy can be determined.

The $\underline{k}$-space position of the energy minimum (band edge point) is found by taking the derivative of Eq. 3.6 with respect to x and setting it equal to zero.

$$K_{x_{min}} = \frac{1}{\hbar} \left[m_{\parallel} V^2 - \frac{\left(\Xi_{u'} e_4 \right)^2}{V^2} \right]^{1/2} \quad . \tag{3.8}$$

Hensel and Hasegawa[3-6] have estimated ΔE at 0.5ev and $\Xi_{u'}$ at 5.7ev. $K_{x_{min}}$ can therefore be plotted as a function of the shear strain, e_4 (see Fig. 3.5). The strain level at which the band edge reaches the symmetry point is

$$\left| e_4 \right| = \frac{\Delta E}{2 \Xi_{u'}} \quad . \tag{3.9}$$

Therefore, for strains below this critical strain, the (100) valley minimum is

$$E_{c_1} = \frac{\Delta E}{4} + \Xi_u \; e_1 + \Xi_d \; (e_1 + e_2 + e_3) - \frac{\left(\Xi_{u'} e_4 \right)^2}{\Delta E} \quad . \tag{3.10}$$

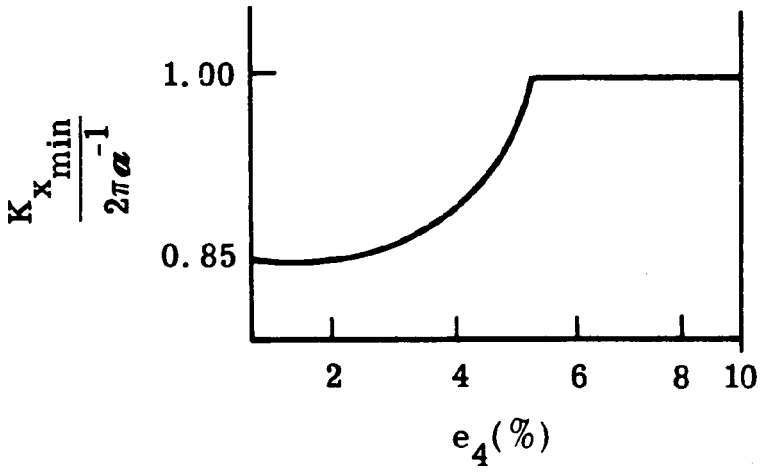


Fig. 3.5 Variation of Band Edge Point as Measured for the Origin in the (100) Direction with Respect to Shear Strain e_4 [After Wortman[3-11].]

Deformation potential coefficients. In order to numerically evaluate the shift in the energy levels, values for the various deformation potential coefficients are required. A number of investigators (see Table 3. 1) have determined the value of some of the coefficients on the basis of piezoresistance and cyclotron resonance experiments. Measurements of the elastic constants of Si [3-2, 3-11, 3-12] have also been used to estimate the deformation potential coefficients. Kleinman et al. [3-7, 3-8, 3-9] have used a knowledge of the electronic wave function for pure silicon to calculate the coefficients (see Table 3. 1). It must be pointed out, however, that these coefficients are known to vary with impurity concentration. Table 3. 2 shows the shear deformation potential coefficient for various impurity concentrations in p-type Si. The spread in the values of the coefficients is an indication of the uncertainty which will appear in the later calculations of the strain dependent barrier height.

Change in the energy gap. Wortman et al. [3-13] have calculated the change of energy levels in Si for hydrostatic, uniaxial (100), uniaxial (111), and uniaxial (110) compressional stresses. Kleinman's theoretical values for the deformation potential coefficients are used in this calculation since they are a consistent set of values. The results of their computations are shown in Table 3. 3.

Table 3.1

Deformation Potential Coefficients (ev/unit dilation) for Si. (Kleinman's theoretical values are shown in brackets.)

D_d	[-2.09]
D_u	2.04[a], [3.74]
$D_{u'}$	2.68[a], [4.23]
Ξ_d	[-4.99]
Ξ_u	11[b], 8.3[c], 8.5[d], [9.57]
$\Xi_{u'}$	5.7[e]
$D_d - \Xi_d + \frac{1}{3}\Xi_u$	-1.44[f], [-0.30]

a. J. C. Hensel and G. Feher, Phys. Rev. 129, 1041 (1963).

b. D. K. Wilson and G. Feher, Phys. Rev. 124, 1068 (1961).

c. J. E. Aubrey, W. Gubler, T. Henningsen and S. H. Koenig, Phys. Rev. 130, 1667 (1963).

d. I. Balslev, Solid State Comm. 3, 213 (1965).

e. J. C. Hensel and H. Hasegawa, paper presented at the International Conference on the Physics of Semiconductors, Paris, July 1964, and private communications.

f. W. Paul, J. Phys. Chem. Solids 8, 196 (1959).

Table 3.2

Values of the Shear Deformation Potential Coefficient D_u, for Boron Doped Si as a Function of Doping Concentration. [After Wortman[3-10].]

Concentration (cm^{-3})	D_u,(ev)
1.4×10^{16}	8.5[b]
2.5×10^{18}	30[a]
3.2×10^{18}	5.8[b]
1.0×10^{19}	13[c]
1.1×10^{20}	11.8[b]

a. W. P. Mason and T. B. Bateman, Phys. Rev. Letters 10, 151, 1 March 1963.

b. P. Csavinsky and Norman G. Einspruch, Phys. Rev. 132, 2434 (1963).

c. W. P. Mason and T. B. Bateman, Phys. Rev. 134, A1387 (1964).

Table 3.3

Calculated Change in Energy Levels in ev x σ x 10^{-12} cm^2/dyn of Si for Hydrostatic, Uniaxial [100], Uniaxial [111] and Uniaxial [011] Compression Stresses.

Stress Tensor / Change In Level	100 010 001	100 000 000	111 111 111	000 011 011
$\Delta\Gamma_{25'}, J = \frac{3}{2}$	3.55	+5.17, -1.73	+4.88, -3.45	+4.03, -2.58
$\Delta X_1[100]$	1.86	-5.66	+7.25, -6.03	+13.74, -6.20
$\Delta X_1[010]$	1.86	3.76	+7.25, -6.03	-0.95
$\Delta X_1[001]$	1.86	3.76	+7.25, -6.03	-0.95
ΔE_g	-0.30(-1.5)[a]	-10.83	-10.9	-10.2

[a]Measured value: see W. Paul, J. Phys. Chem. Solids 8, 196 (1959). [After Wortman et al.[3-13].]

3.1.2 Carrier Concentrations. For nondegenerate semiconductors where Maxwell-Boltzmann statistics apply, the electron density associated with a single ellipsoidal energy surface at a band edge is

$$n = 2\left(\frac{2\pi kT}{\hbar^2}\right)^{3/2} m_c^{3/2} \exp\left(-\frac{E_c - E_F}{kT}\right) \qquad (3.12)$$

where m_c is the effective mass of the electron in the conduction

band minimum. For a multivalley semiconductor such as silicon, the total conduction band electron density is the sum of the densities associated with each minimum. Silicon has six minima in the (100) k-space directions. In the unstrained crystal the effective mass of the electrons in the separate minima are equal. In the strained crystal, pairs of minima are affected identically (i.e., when stress is applied, the (100) minimum is changed in the same way as the ($\bar{1}00$) minimum). Therefore, the electron density for silicon can be written as

$$n = 4\left(\frac{2\pi kT}{h^2}\right)^{3/2}\left[m_{c_1}^{3/2}\exp\left(-\frac{E_{c_1}-E_F}{kT}\right)+m_{c_2}^{3/2}\exp\left(-\frac{E_{c_2}-E_F}{kT}\right)+m_{c_3}^{3/2}\exp\left(-\frac{E_{c_3}-E_F}{kT}\right)\right] \tag{3.13}$$

where c_1, c_2, c_3 refer to the energy minima in the (100), (010) and (001) k-space directions respectively.

When the crystal is strained, the conduction band minima are shifted and distorted as described above. The distortion of the energy surfaces implies that the effective masses will not be equal in the presence of strain. Wortman[3-10] has shown that the ratio of the strained effective mass to the unstrained effective mass of the conduction band electrons is a function only of shear strain. Moreover, for shear strains of less than 2 percent, there is less than a 10 percent

change in the effective mass. Since the effective mass enters into the calculation for n as a 3/2 power while changes in the energy level enter in exponentially, strain dependent changes in the effective masses are neglected.

The conduction band minima and the valence band maxima shift with stress. Thus, in general, the Fermi level must also shift with the application of stress. The stress dependent electron density can now be written as

$$n = n_o\left(\frac{1}{3}\right) \exp\left(\frac{\Delta E_F}{kT}\right)\left[\exp\left(\frac{\Delta E_{c_1}}{kT}\right) + \exp\left(\frac{\Delta E_{c_2}}{kT}\right) + \exp\left(\frac{\Delta E_{c_3}}{kT}\right)\right] \quad (3.14)$$

where n_o is the unstrained electron density, ΔE_F is the change in the Fermi level and ΔE_{C_i} $(i = 1, 2, 3)$ are the changes in the conduction band minima.

The hole density, p, at zero stress is given by

$$p = 2\left(\frac{2\pi kT}{\hbar^2}\right)^{3/2}\left[m_{v_1}^{3/2} \exp\left(-\frac{E_F - E_{v1}}{kT}\right) + m_{v_2}^{3/2} \exp\left(-\frac{E_F - E_{v2}}{kT}\right) + m_{v_3}^{3/2} \exp\left(-\frac{E_F - E_{v3}}{kT}\right)\right] \quad (3.15)$$

where v_1 and v_2 refer to the $\Gamma_{25'}$, $(J = 3/2)$ heavy and light hole bands respectively and v_3 refers to the $\Gamma_{25'}$, $(J = 1/2)$ band. The m's are the effective masses of the holes in the various bands. Because of the smaller mass and lower energy, the density of the holes in the $\Gamma_{25'}$, $(J = 1/2)$ level constitute less than 20 percent of the total hole

density. If the holes in this level are neglected, Eq. 3.15 can be written as

$$p_o = 2\left(\frac{2\pi kT}{\hbar^2}\right)^{3/2} (m_v^*)^{3/2} \left[\exp\left(-\frac{E_F - E_{v_1}}{kT}\right) + \exp\left(-\frac{E_F - E_{v_2}}{kT}\right)\right] \tag{3.16}$$

where

$$m_v^* = \left(m_{v_1}^{3/2} + m_{v_2}^{3/2}\right)^{2/3} \tag{3.17}$$

Since E_{v_1} and E_{v_2} are equal at zero stress, the hole density in the presence of stress can be written as

$$p = p_o \exp\left(-\frac{\Delta E_F}{kT}\right)\left[\left(\frac{m_{v_1}}{m_v^*}\right)^{3/2} \exp\left(\frac{\Delta E_{v_1}}{kT}\right) + \left(\frac{m_{v_2}}{m_v^*}\right)^{3/2} \exp\left(\frac{\Delta E_{v_2}}{kT}\right)\right]. \tag{3.18}$$

Equations 3.14 and 3.18 are valid regardless of the doping of the crystal.

When compressional stress is applied, the band gap decreases and the density of intrinsic carriers increases. If the doping density is high enough*, the density of the majority carriers will remain essentially constant. Therefore, for an n-type crystal, it can be shown from Eq. 3.14 that

---

*This condition is defined in Eq. 3.23.

$$\exp\left(-\frac{\Delta E_F}{kT}\right) = \exp\left(-\frac{\Delta E_{c1}}{kT}\right) + \exp\left(-\frac{\Delta E_{c2}}{kT}\right) + \exp\left(-\frac{\Delta E_{c3}}{kT}\right) \quad . \quad (3.19)$$

Substituting this into Eq. 3.18

$$\frac{p_n}{p_o} = \left(\frac{1}{3}\right)\left[\left(\frac{m_{v1}}{m_v^*}\right)^{3/2} \exp\left(\frac{\Delta E_{v1}}{kT}\right) + \left(\frac{m_{v2}}{m_v^*}\right)^{3/2} \exp\left(\frac{\Delta E_{v2}}{kT}\right)\right] \cdot \left[\exp\left(-\frac{\Delta E_{c1}}{kT}\right) + \exp\left(-\frac{\Delta E_{c2}}{kT}\right) + \exp\left(-\frac{\Delta E_{c3}}{kT}\right)\right] \quad (3.20)$$

where p_n is the strain dependent minority carrier density and p_{no} is the zero strain minority carrier density. If a similar calculation is performed for a p-type crystal, the ratio of the electron density with stress to the electron density with zero stress is the same expression as the right-hand side of Eq. 3.20.

A new quantity, $\gamma(\sigma)$, can now be defined as

$$\gamma(\sigma) = \frac{p_n}{p_{no}} = \frac{n_p}{n_{po}} \quad . \quad (3.21)$$

For hydrostatic stress, $\Delta E_{c_1} = \Delta E_{c_2} = \Delta E_{c_3}$ and

$$\gamma(\sigma) = \exp\left(-\frac{\Delta E_g}{kT}\right) \quad . \quad (3.22)$$

Figure 3.6 shows a plot of $\gamma(\sigma)$ versus stress for several directions of uniaxial compression. These curves are calculated using Kleinman's theoretical values for the deformation potential coefficients.

Conditions for the validity of the above can now be stated in terms of the result of the analysis. For silicon, Eq. 3.21 is valid if

$$\gamma \cdot p_n << \left| N_D - N_A \right| \qquad \text{(n-type Si)}$$
$$\gamma \cdot n_p << \left| N_D - N_A \right| \qquad \text{(p-type Si)} \tag{3.23}$$

When Eq. 3.23 is satisfied, the p-n product in the presence of stress becomes

$$n_i^2 = np = n_o p_o \gamma(\sigma) = n_{io}^2 \gamma(\sigma) \tag{3.24}$$

where n_i is the strain dependent intrinsic carrier density and n_{io} is the zero strain intrinsic carrier density.

3.1.3 One-Dimensional, Stress Dependent Energy Band Diagram. On the basis of the detailed analysis above, the stress dependence of the simple, one-dimensional energy band diagram can be shown. For hydrostatic or uniaxial stresses such that Eq. 3.23 is always satisfied, the change in the energy gap can be found directly from Table 3.3 or from Eqs. 3.2 and 3.10 after suitable coordinate transformations. Given the zero stress band diagram, the stressed band diagram is obtained by shifting the minority carrier band extremum by an amount ΔE_g.

For example, consider n-type silicon. If the zero stress band diagram is as shown in Fig. 3.7(a) and if a compressive uniaxial stress, σ, is applied along the (111) direction, the stress dependent energy band

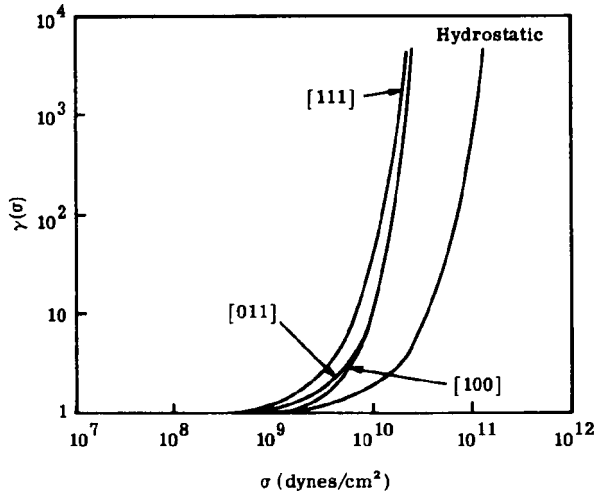


Fig. 3.6 Ratio of Minority Carrier Density with Stress to the Unstressed Minority Carrier Density $\gamma(\sigma)$ as a Function of Stress in Si. Values are Given for Hydrostatic, [100], [111], and [001] Uniaxial Compression Stresses. [After Wortman et al.[3-14].]

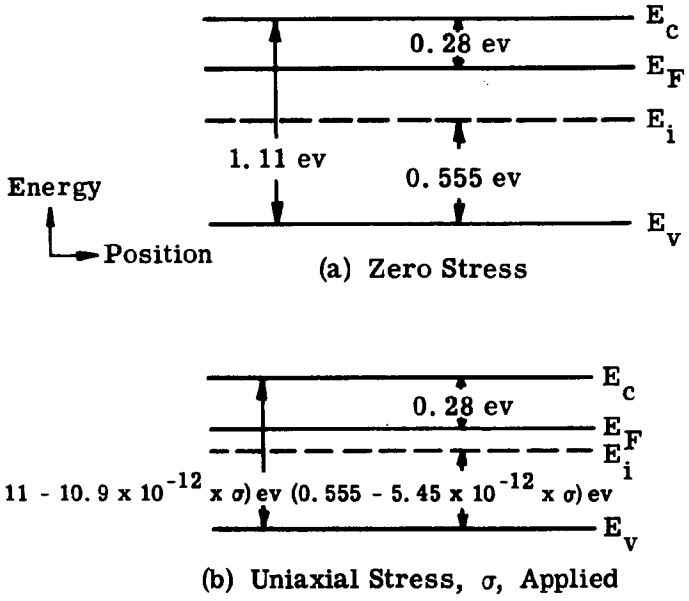


Fig. 3.7 One-Dimensional Energy Band Diagrams for Si.

diagram is as shown in Fig. 3.7(b). The quantity, $E_C - E_F$, is constant. The shift in the conduction band edge and the valence band edge are effectively taken into account by raising the valence band edge by ΔE_g.

3.1.4 Stress Dependence of the Barrier Height. The same arguments that were used in the preceding subsection for determining the one-dimensional stress dependent energy band diagram for the bulk can now be used to determine the stress dependence of the barrier height. In the presence of stress, the band gap in the space-charge region must shift. However, in the space-charge region, the majority carrier density is not high enough to mask the addition of intrinsic carriers. Thus, the changing band gap must generally be accounted for by a shift in both the conduction and valence band extrema.

At the interface the band bending may be such that an inversion layer is formed (i.e., $E_i(x = 0) > E_F$ for n-type bulk). This inversion layer may, in turn, be such that the density of minority carriers at the interface will be insensitive to the additional intrinsic carriers. (This is the case for the gold to n-type silicon contacts considered in Chapter IV.) Therefore, by analogy to Eq. 3.23, if

$$\gamma(\sigma)\, n_{so} \ll p_{so} \quad \text{(for n-type bulk)}$$

or , (3.25)

$$\gamma(\sigma)\, p_{so} \ll n_{so} \quad \text{(for p-type bulk)}$$

at the interface, the band gap changes appear as a shift in the bulk majority carrier band while the bulk minority carrier band is fixed. (See Fig. 3.8.)

Note that the condition stated in Eq. 3.25 must be satisfied for maximum stress sensitivity of the barrier height. If this condition is not satisfied, then both bands at the interface must be shifted to account for ΔE_g and the stress sensitivity of the barrier height is reduced.

3.2 Stress Dependence of Majority Carrier (Schottky) Current

The majority carrier current is

$$I_n = a A T^2 \exp\left(\frac{-\varphi_B}{kT}\right) \left[\exp\left(\frac{qU}{kT}\right) - 1\right] \qquad (2.15)$$

where

$$A = \frac{4\pi q m k^2}{h^3} \quad . \qquad (3.26)$$

Since the barrier height, φ_B, enters into this expression exponentially, changes in φ_B will have a far greater effect on the current than will change in the effective mass. Therefore Richardson's constant, A, is assumed to be independent of stress. The maximum stress sensitivity of the barrier height occurs when Eq. 3.25 is satisfied and when the stress is applied along the (111) direction. (See Table 3.3.) In this case the stress dependent Schottky current is

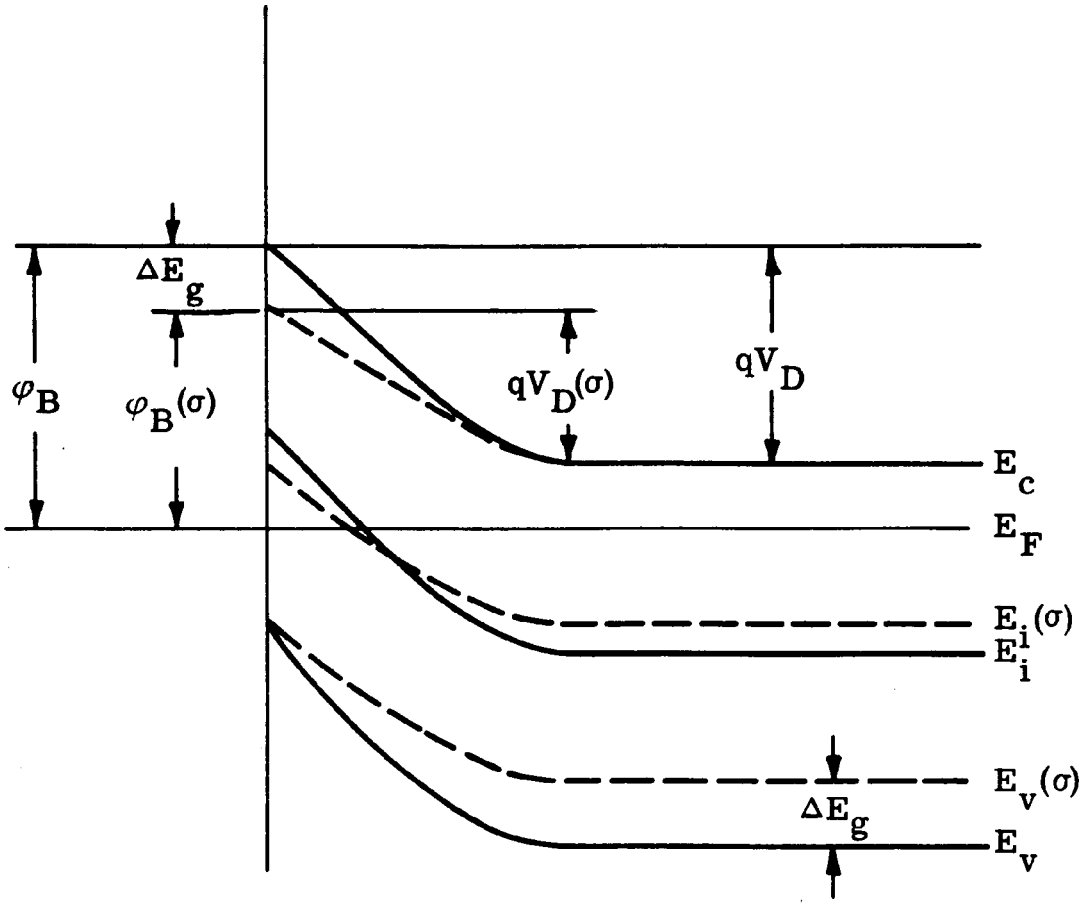


Fig. 3. 8 Energy Band Diagram of Metal-Semiconductor Contact.

Without stress (solid lines)
With compressional stress (dotted lines)

$$I_n(\sigma) = I_{no} \exp\left(- \frac{1.09 \times 10^{11} \times \sigma}{kT}\right) \left[\exp\left(\frac{qU}{kT}\right) - 1\right] \qquad (3.27)$$

where I_{no} is the saturation current at zero stress.

A family of stress dependent Schottky barrier diode volt-ampere curves can now be drawn for this maximum stress sensitive case. (See Fig. 3.9.) Note that these curves have been calculated assuming that at high-forward current the voltage drop across the spreading resistance[3-15] of the semiconductor, R_s, must be taken into account. Thus

$$U = V_a - I R_s \qquad (3.28)$$

where V_a is the potential applied to the terminals of the diode and

$$R_s = \frac{\rho}{4 R_c} \qquad (3.29)$$

where ρ is the bulk resistivity of the semiconductor and R_c is the radius of the metal contact. The various curves are labeled with the stress and "force" (grams) applied to the contact assuming a simple force over area computation for the stress.

3.3 Stress Dependence of Minority Carrier Current

The minority carrier current is

$$I_p = a q p_n \sqrt{\frac{D_p}{\tau_p}} \left[\exp\left(\frac{qU}{kT}\right) - 1\right]. \qquad (3.23)$$

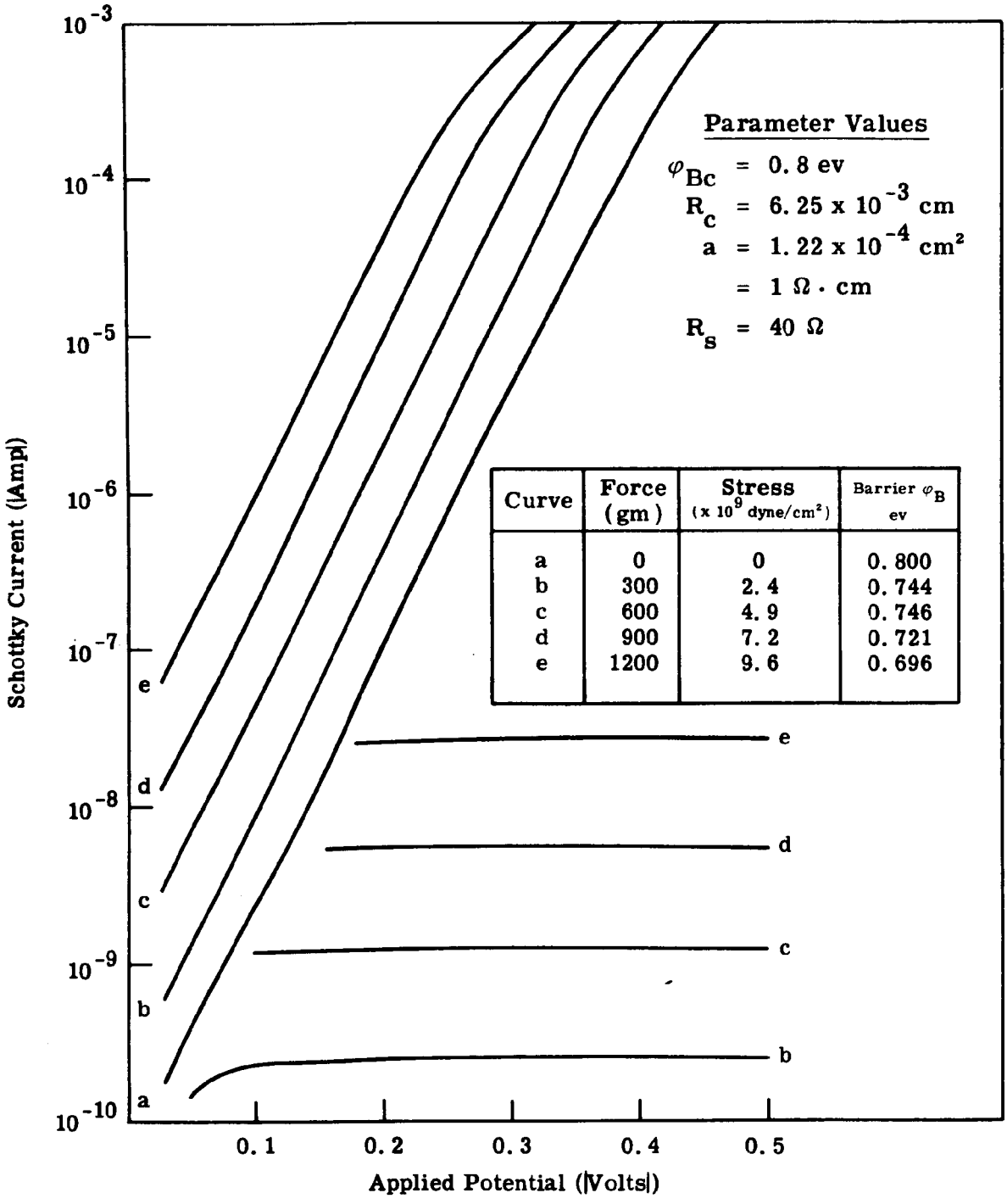


Fig. 3.9 Schottky Current Volt-Ampere Characteristic with Stress Dependent Barrier Height.

For maximum stress sensitivity, assume that the condition of Eq. 3.23 is satisfied. The minority carrier density in the bulk in the presence of stress is

$$p_n(\sigma) = p_{no} \exp\left(-\frac{\Delta E_g}{kT}\right) \tag{3.30}$$

where p_{no} is the zero stress minority carrier density in the bulk. The quantities, D_p and τ_p, are not as sensitive to stress as is the hole density. Matukura[3-16] has measured the lifetime of minority carriers in stressed silicon p-n junctions and has shown that the minority carrier lifetime decreases by about 20 percent for stress in the range of 10^{10} to 10^{11} dynes/cm^2. The diffusion coefficient, D_p, is expected to vary as the mobility varies according to the Einstein relation. On the basis of piezoresistivity measurements, Wortman[3-10] has shown that the changes in the mobility are small compared to changes in the minority carrier density.

Thus the stress dependent minority carrier current can be written as

$$I_p(\sigma) = I_{po}\,\gamma(\sigma)\left[\exp\left(\frac{qU}{kT}\right) - 1\right] \tag{3.31}$$

where I_{po} is the unstressed minority carrier saturation current.

Note that this current has the same stress variation as that shown for the Schottky current in Eq. 3.27.

3.4 Stress Dependence of the Space-Charge Recombination Current

The space-charge recombination current was shown to be

$$I_r = \frac{a\, q\, n_i^2\, W \left[\exp\left(\frac{qU}{kT}\right) - 1\right]}{(\tau_{po}\, n_1 + \tau_{no}\, p_1) + (\tau_{no} + \tau_{po})\, n_i \exp\left(\frac{qU}{2kT}\right)} \tag{2.44}$$

where

$$n_1 = n_i \exp\left(\frac{E_t - E_i}{kT}\right) \tag{2.32}$$

and

$$p_1 = n_i \exp\left(\frac{E_i - E_t}{kT}\right) . \tag{2.33}$$

If

$$\tau_{no} = \tau_{po} \tag{3.32}$$

the space-charge recombination current can be written as

$$I_r = \frac{a\, q\, n_i\, W \left[\exp\left(\frac{qU}{kT}\right) - 1\right]}{2\, \tau_{no} \left[\exp\left(\frac{E_t - E_i}{kT}\right) + \exp\left(\frac{E_i - E_t}{kT}\right) + \exp\left(\frac{qU}{2kT}\right)\right]} \tag{3.33}$$

The stress dependence of n_i has been shown in Eq. 3.24 to be:

$$n_i(\sigma) = n_{io}\, \gamma^{1/2}(\sigma) . \tag{3.32}$$

The barrier width, W, depends on a fractional power of the diffusion potential.

$$W = \sqrt{\frac{2\epsilon}{q N_D} (V_D - U)} , \qquad (2.10)$$

implying that changes in V_D produce small changes in W. Therefore, the barrier width is assumed to be constant in the presence of stress. The lifetime, $\tau_{no} = \tau_{po}$, as discussed in the previous section, is also assumed to be constant.

The stress dependence of the quantity, $E_t - E_i$, is extremely difficult to assess, either theoretically or experimentally. The physical origin of the traps associated with the E_t may be crystal lattice defects or impurity atoms located interstitially or substitutionally in the lattice. Just how the energy levels associated with these traps will vary when stress is applied to the crystal is not known. For the time being, consider three alternative assumptions: 1) $E_t - E_i$ is constant, 2) $E_t - E_i$ increases, or 3) $E_t - E_i$ decreases when compressive stress is applied to the crystal. (In Chapter IV, after the experimental data have been presented, these assumptions will be discussed in terms of what may be happening physically in the stressed crystal.)

1) Assume that the energy level of the traps is fixed with respect to the intrinsic energy level,, then the stress dependence of the space-charge recombination current is due solely to the stress

dependence of n_i. Figure 3.10 shows a family of volt-ampere curves for the space-charge recombination current on the basis of this assumption. The values for the other quantities appearing in the equation for the current are shown in the figure. (The character of the stress dependence of this figure as well as of Figs. 3.9 and 3.11 will be used to suggest the interpretation of the experimental data presented in Chapter IV.)

2) Assume that the trap energy moves away from the intrinsic energy when compressive stress is applied, then the denominator of Eq. 3.33 would increase for increasing stress. Therefore, this current would have a tendency to remain constant (if $E_t - E_i$ is as sensitive to stress as E_g) or to decrease (if $E_t - E_i$ is more sensitive to stress than E_g). Since it is well known that the current through a metal-semiconductor contact increases with increasing compressive stress, this assumption is probably incorrect.

3) Assume that the energy level of the traps moves toward the intrinsic level as compressive stress is applied, then the denominator of the expression decreases and the current increases. In addition, the shape of the forward characteristic with this assumption will be different than the shape of the characteristic in the case where the trap energy is fixed relative to the intrinsic energy. This may be seen by comparing Fig. 3.11 with Fig. 3.10. As will be shown in Chapter IV, the shape of the experimental volt-ampere characteristic in the low forward bias region is much like that shown in Fig. 3.11.

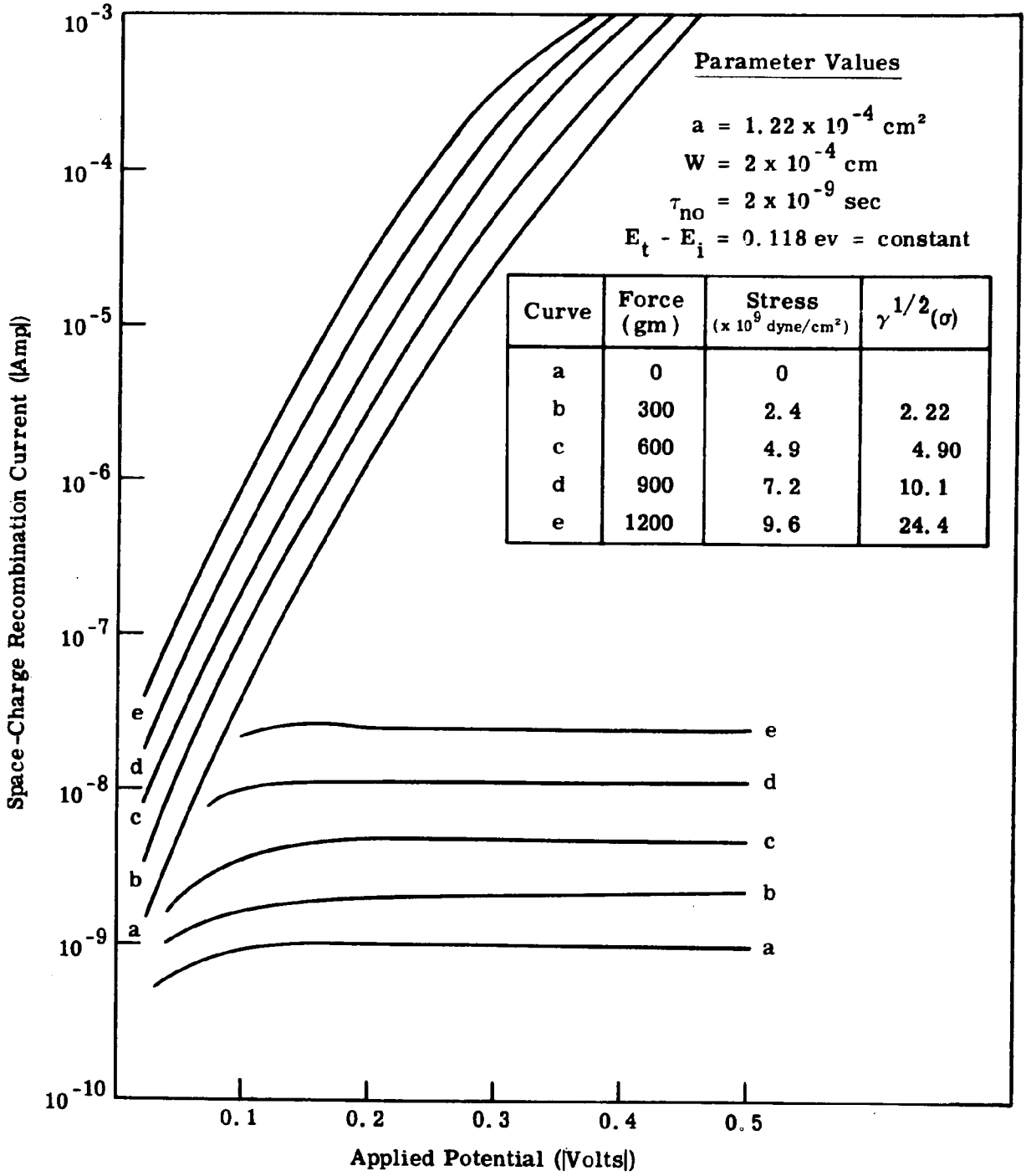


Fig. 3.10 Space-Charge Recombination Current Volt-Ampere Characteristic with Stress Dependent n_i and Constant $E_t - E_i$.

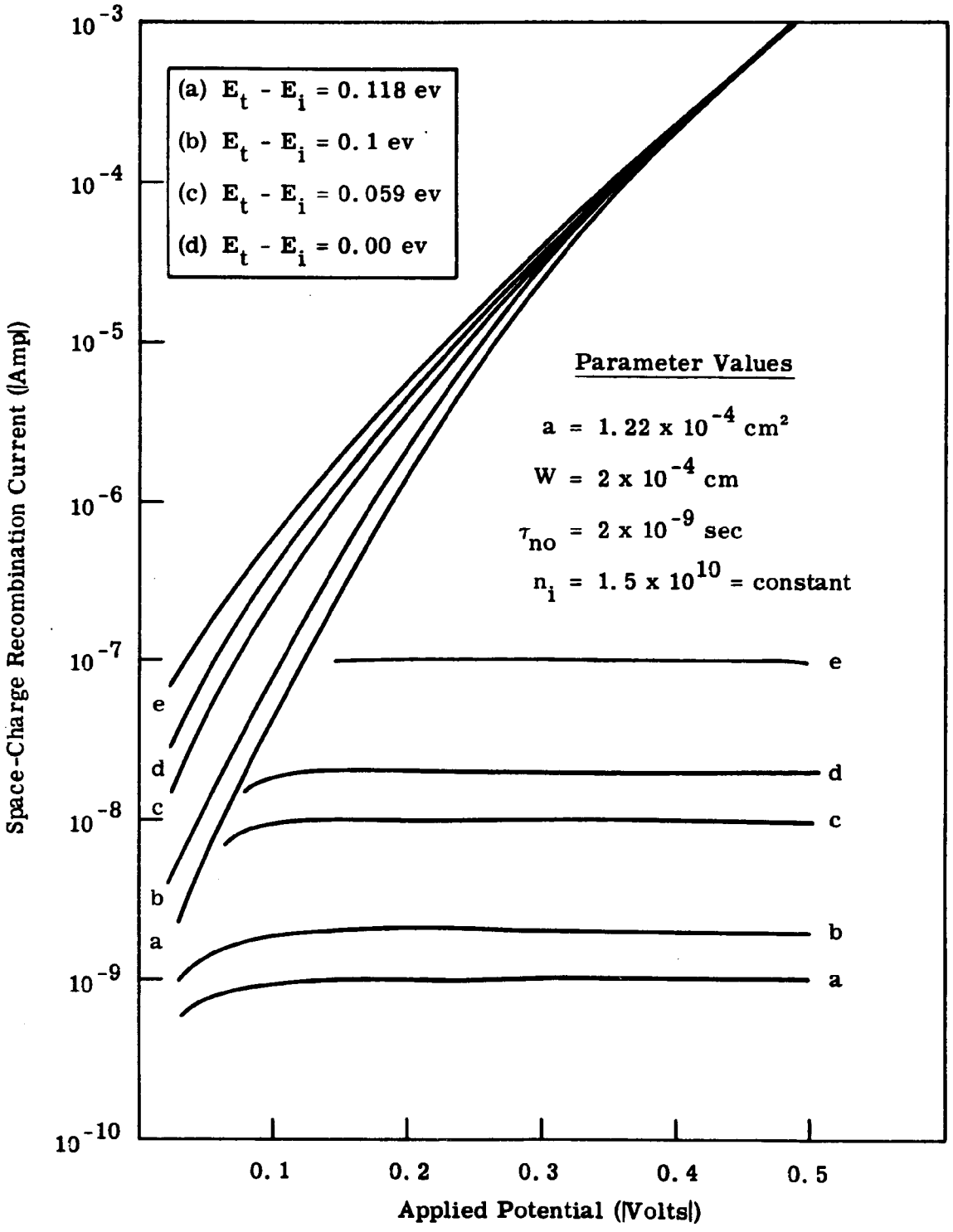


Fig. 3.11 Space-Charge Recombination Current Volt-Ampere Characteristic with Constant n_i and Various Values for $E_t - E_i$.

The reader should bear in mind that the expression for the space-charge recombination current was derived by assuming that the traps were uniformly distributed throughout the semiconductor and by also assuming that these traps could be characterized by a single energy level, E_t. While this may be a gross approximation to the real case, the consideration of a single effective trap energy is sufficient for the purpose of study.

3.5 Stress Dependence of Surface Recombination Current

The surface recombination current is

$$I_{rs} = \frac{a\, q\, n_i^2 \left[\exp\left(\frac{qU}{kT}\right) - 1\right]}{\frac{n_1}{v_{po}} + \frac{p_{so} + p_1}{v_{no}} + \frac{n_i}{v_{po}} \exp\left(\frac{qU}{kT}\right)} \quad . \tag{2.47}$$

The quantities n_1 and p_1 have been discussed in the previous section. The same alternative assumptions can be made in this case. The variation of n_i has also been discussed above (see Eq. 3.24). The stress dependence of the surface recombination velocities, v_{po} and v_{no}, remain to be discussed here.

These velocities can be expressed as[3-17]

$$\begin{aligned} v_{no} &= N_{ss} \sum_n v_{th} \\ v_{po} &= N_{ss} \sum_p v_{th} \end{aligned} \tag{3.33}$$

where N_{ss} is the density of surface states, $\sum_n$ $\sum_p$ is the capture cross section of these states for electrons (holes) and v_{th} is the thermal velocity of the electrons (holes) as they cross the interface. Again there is no information available to determine how these quantities will vary when stress is applied to the crystal.

If one assumes that the surface state density and the capture cross sections vary only slightly in the presence of compressive stress, the stress sensitive surface recombination current can be written as

$$I_{rs} = \frac{a\, q\, n_{io}^2\, \gamma(\sigma) \left[\exp\left(\frac{qU}{kT}\right) - 1 \right]}{\frac{n_1(\sigma)}{v_{po}} + \frac{p_{so} + p_1(\sigma)}{v_{no}} + \frac{n_{io}\, \gamma^{1/2}(\sigma)}{v_{po}} \exp\left(\frac{qU}{kT}\right)} \qquad (3.37)$$

3.6 Summary

In this chapter the effect of a crystalline strain on the energy bands of silicon has been discussed. The stress dependent changes which are expected in the bulk are used to deduce the effect of stress on the barrier height of a metal-silicon contact. As discussed above, the information required to completely determine the effect of stress on each of the current components is not available. In particular, information concerning how stress affects the trap energy levels and the surface recombination velocities is not available. It was arbitrarily assumed that the stress dependent variation on the surface recombination velocities can be neglected.

With the various assumptions and/or conditions stated in the above sections, the stress dependent current components are listed below for quick reference.

1) Majority Carrier (Schottky) Current

$$I_n(\sigma) = I_{no}\,\gamma(\sigma)\left[\exp\left(\frac{qU}{kT}\right) - 1\right] \tag{3.38}$$

2) Minority Carrier Current

$$I_p(\sigma) = I_{po}\,\gamma(\sigma)\left[\exp\left(\frac{qU}{kT}\right) - 1\right] \tag{3.39}$$

3) Space-Charge Recombination Current

$$I_r(\sigma) = \frac{a\,q\,n_{io}\,\gamma^{1/2}(\sigma)\left[\exp\left(\frac{qU}{kT}\right) - 1\right]}{2\,\tau_{no}\left[\exp\left(\frac{E_t - E_i}{kT}\right) + \exp\left(\frac{E_i - E_t}{kT}\right) + \exp\left(\frac{qU}{2kT}\right)\right]} \tag{3.40}$$

4) Surface Recombination Current

$$I_{rs}(\sigma) = \frac{a\,q\,n_{io}^2\,\gamma(\sigma)\left[\exp\left(\frac{qU}{kT}\right) - 1\right]}{\frac{n_1(\sigma)}{v_{po}} + \frac{p_{so} + p_1(\sigma)}{v_{no}} + \frac{n_{io}\,\gamma^{1/2}(\sigma)}{v_{po}}\exp\left(\frac{qU}{kT}\right)} \tag{3.41}$$

CHAPTER IV

EXPERIMENTAL RESULTS AND COMPARISON WITH THEORY

In this chapter a brief description of the techniques used to fabricate the experimental metal-semiconductor diodes is presented*. The data acquisition system as well as the logic of the data analysis is described. At zero stress, the experimental volt-ampere characteristic is shown to be essentially that of a Schottky Barrier diode. The application of compressional stress to the contact is shown to cause a large increase in the space-charge recombination current.

4.1 The Experimental Setup

4.1.1 Choice of the Experimental Diode. The particular type of metal-semiconductor diode which is used to experimentally investigate the stress effect was chosen on the basis of the following considerations:

1) Type of Contact. The effect of stress on rectifying contacts is most pronounced for a point contact. However, in the case of point contacts, the area of the contact is extremely difficult to determine. Moreover, since the contact area changes when force is applied to the

---

*The author would again like to acknowledge Tecumseh Products Company for making their Research Laboratory facilities available to him.

point, the data are more difficult to interpret. Also, the problem of oxide growth on the surface of the semiconductor may force the consideration of a thin insulating region at the interface, thus raising further difficulties in the interpretation of the data. Because of such problems with the point contact, an evaporated type of metal-semiconductor contact is chosen.

2) Barrier Height. It is expected, on the basis of the band shifting model presented in Chapter III, that the barrier height will be most sensitive to stress when Eq. 3.25 is satisfied. This equation will probably be satisfied for any of those semiconductors in which the barrier height is on the order of $\frac{2}{3}$ E_g (see Fig. 2.3).

3) Strain Dependent Hamiltonian and Deformation Potential Coefficients. At the time this study was initiated, it was expected that the shift in the volt-ampere characteristic could be explained on the basis of stress dependent changes in the barrier height of the contact. It was, therefore, imperative to have available the stress dependent Hamiltonian and numerical values for the deformation potential coefficients. These were readily available for the Group IV semiconductors[4-1, 4-2, 4-3, 4-4], so the choice of which semiconductor to use was narrowed to two—germanium and silicon.

4) Knowledge of the Zero Stress Characteristic. Since this study is primarily concerned with the effect of mechanical stress on the volt-ampere characteristic of metal-semiconductor contacts, it

is important to choose an experimental configuration whose characteristic at zero stress is known to fit some theoretical model. The evaporated gold contact on n-type silicon is known to form a good Schottky Barrier[4-5, 4-6, 4-7, 4-8]. In addition, it has been shown that gold contacts evaporated on chemically cleaned silicon substrates have the same volt-ampere characteristic as gold contacts evaporated on vacuum cleaved silicon substrates[4-9]. Thus experimental contacts with this configuration can be fabricated without the necessity of resorting to vacuum cleaving procedures.

For these reasons the evaporated gold contact on n-type silicon was chosen as the system to be used to experimentally investigate the stress effect. The devices were fabricated by evaporating gold through a metal mask with 0.005 in. diameter openings onto heated, chemically cleaned, n-type silicon substrates. Some mesa diodes were also fabricated using photo-resist processes after the evaporation of the contact. For details of the fabrication process, the reader is referred to Appendix B.

4.1.2 Physical Test Arrangement. A picture of the physical arrangement for testing the diodes is shown in Fig. 4.1. A schematic drawing of this arrangement is shown in Fig. 4.2.

The semiconductor chip, mounted on a header, is attached to an x-y-z micrometer stage. Using a stereo microscope, an evaporated contact is positioned under the stylus and the stage is raised

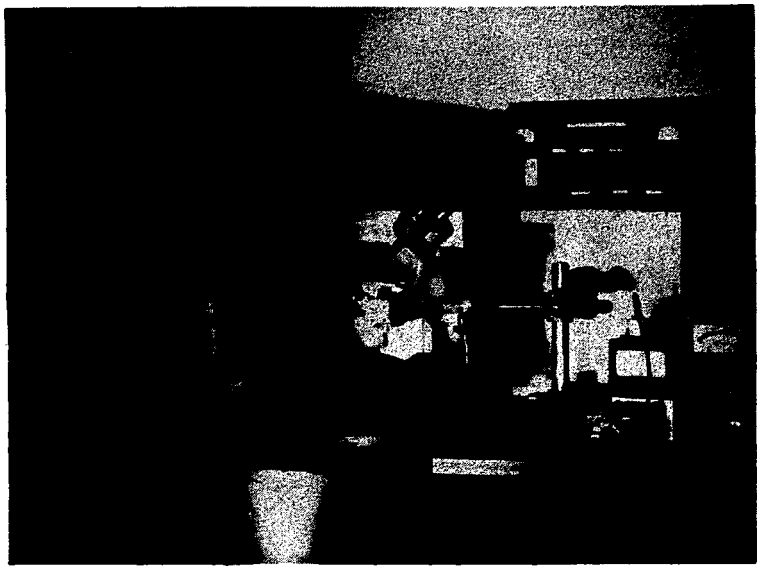


Fig. 4. 1 Photograph of Electrical Test Setup.

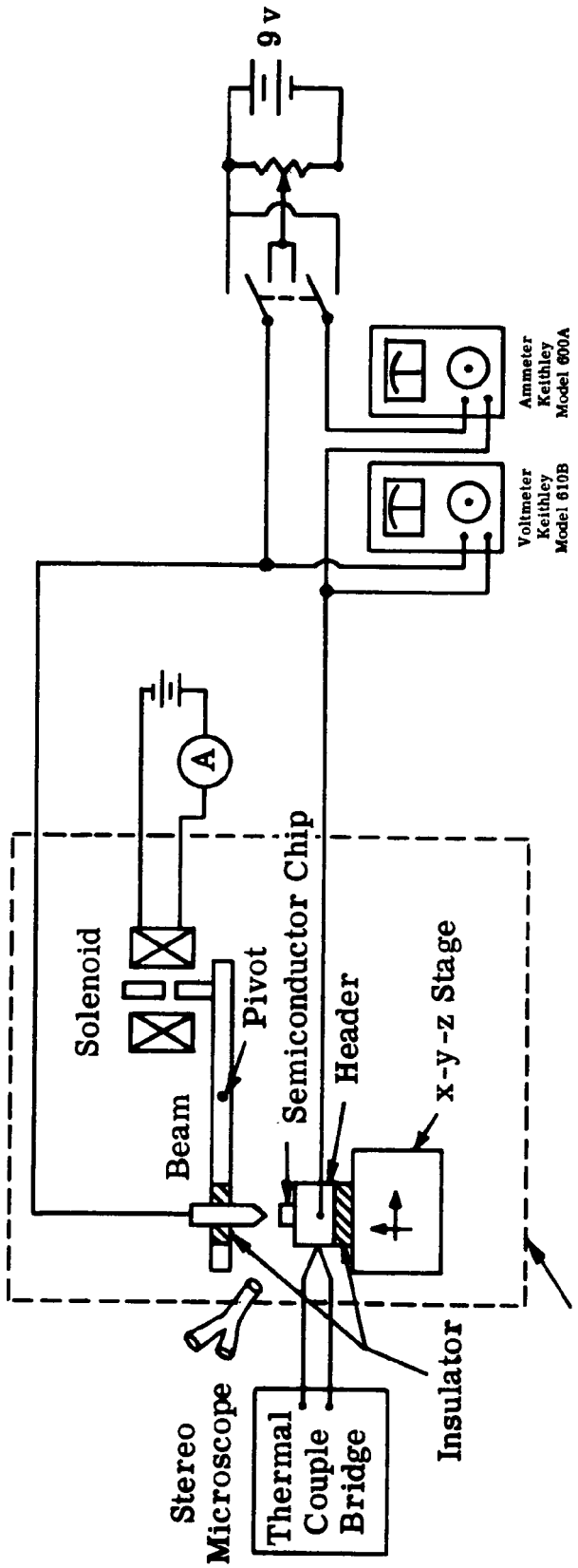


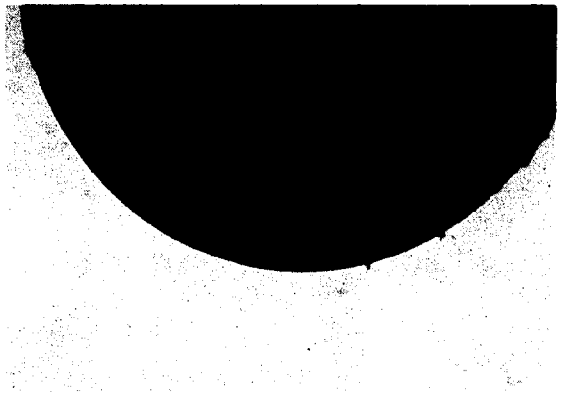
Fig. 4.2 Schematic of Electrical Test Setup.

until electrical contact is made. The header and the stylus are electrically insulated from the stage and the beam respectively. Low leakage coaxial cable is used to interconnect the device with the measuring circuit.

The temperature chamber is an Associated Testing Laboratory Model SLHU-1-LC which has a temperature range from $-100^{o}F$ to $+425^{o}F$. Provision for an artifical atmosphere is also available. In the present study a dry nitrogen atmosphere is used. The chamber has a thermostatic control to maintain the atmosphere at the programmed temperature. Since there is a thermal lag between the temperature of the atmosphere and the temperature of the test fixture, thermalcouple is placed in contact with the header. This thermalcouple is used to determine when the header has come to equilibrium with the atmosphere.

An electrometer is used to measure the diode potential. The high input impedance of the electrometer ($> 10^{13}\ \Omega$) insures that the current through the voltmeter can be neglected at all bias levels. The volt-ampere characteristic is measured at d. c. point by point over the applied potential range -0. 5 volts to +0. 5 volts.

The stress is applied by means of a stylus, beam, and current-calibrated electromagnet as shown in Fig. 4. 2. Figure 4. 3 shows two of the styli that are used in this study.



(a) 0.023 inch Radius of Curvature
Chrome Steel (160 X)



(b) ~ 0.030 inch Radius of Curvature;
~ 0.004 inch Across the "Flat",
303 Stainless Steel (35 X)

Fig. 4.3 Stylus Points.

4.2 Experimental Volt-Ampere Characteristics with Zero Mechanical Stress

As mentioned above the diodes were formed by evaporating gold onto the surface of a silicon chip or wafer. If the diode was tested as fabricated, it is referred to as a planar diode. If, after the evaporation, a photo-resist procedure was used to etch away a few microns of the silicon outside the area of the contact, the diode is referred to as a mesa diode. (The mesa diodes were fabricated because with this configuration an approximately uniaxial stress field can be achieved conveniently.)

Note that all silicon wafers used in this study were oriented with the (111) direction perpendicular to the metal-semiconductor interface.

4.2.1 Planar Diodes. The volt-ampere characteristic of a typical 0.005 inch diameter gold contact to 0.7 Ω-cm, n-type silicon is shown in Fig. 4.4.

Examine the forward characteristic. In the middle range of applied potential, the curve is straight and has a slope of q/η kT where the η for this diode is 1.09. This indicates that the current in this linear range of the forward characteristic is either Schottky current or minority carrier current. The extrapolation to zero bias of this linear portion of the curve yields a saturation current, I_o, of about 10^{-10} amperes.

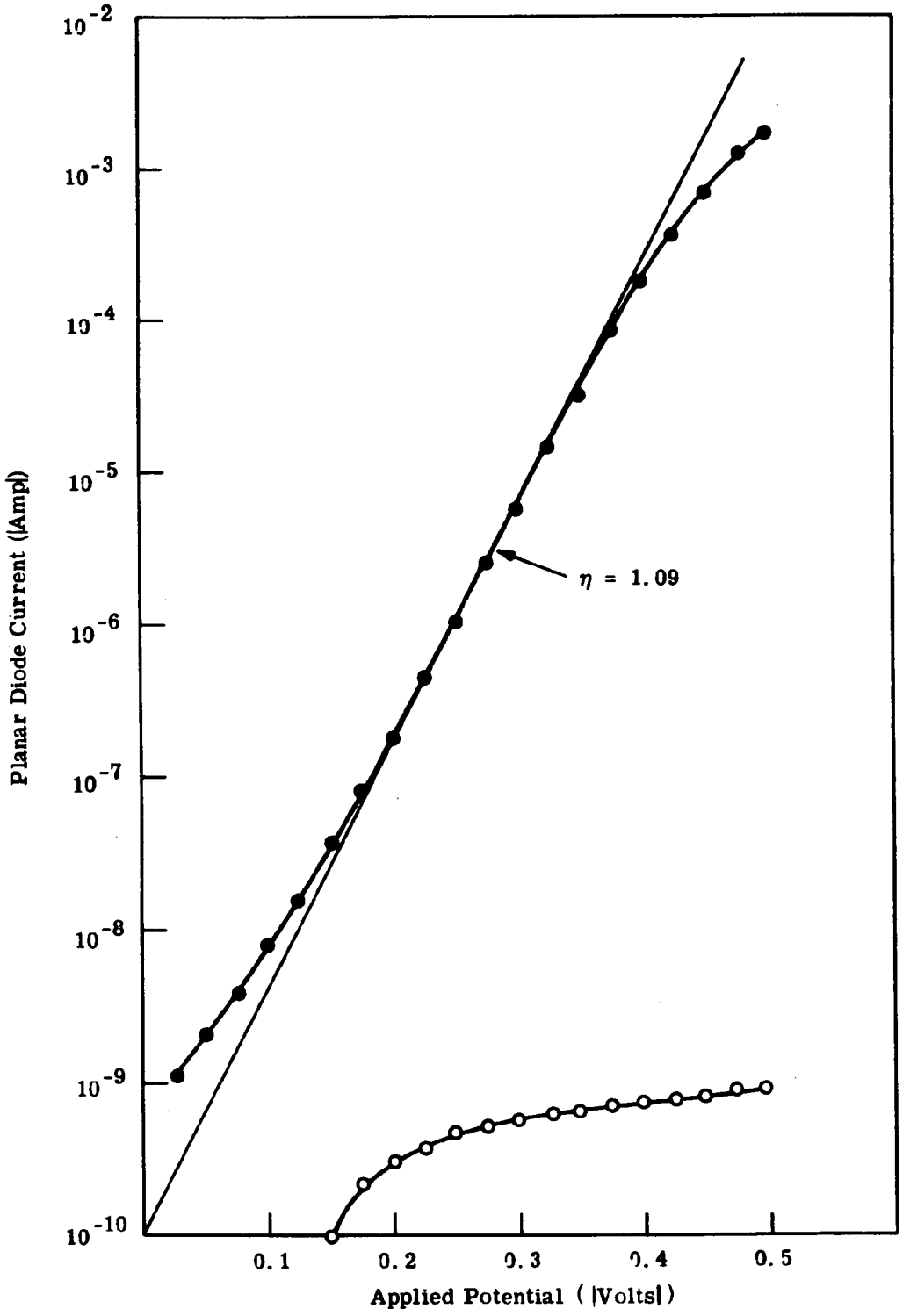


Fig. 4.4 Zero Stress Volt-Ampere Characteristic of Typical Planar Gold-Silicon Contact.

The Schottky saturation current is given by: (see Eq. 2.15)

$$I_{no} = a\,A\,T^2 \exp\left(\frac{-\varphi_B}{kT}\right) . \tag{4.1}$$

If φ_B is taken as 0.8 ev,

$$I_{no} \approx 10^{-11} \text{ amp} \tag{4.2}$$

at room temperature.

The minority carrier saturation current is (see Eq. 2.23)

$$I_{po} = a\,q\,P_n\sqrt{\frac{D_p}{\tau_p}} . \tag{4.3}$$

If τ_p is taken as 10^{-6} seconds

$$I_{po} \approx 10^{-15} \text{ amp} \tag{4.4}$$

Therefore, it appears from the above that the linear range of the forward characteristic is dominated by Schottky current.

The excess current that is present for low forward bias (the difference between the measured current and the extrapolation of the linear portion of the curve) is due to the presence of a recombination current.

Consider first the equation for the surface recombination current (Eq. 2.47 and Eq. 2.48). The maximum value for this current appears at high forward bias and has the form:

$$I_{rs\ max} = a\, q\, n_i\, N_{ss} \sum_p v_{th} \quad . \tag{4.5}$$

If

$$v_{th} = \sqrt{\frac{kT}{2m}} \tag{4.6}$$

$$\sum_p \approx 10^{-15}\ cm^2 \tag{4.7}$$

and

$$N_{ss} \approx 10^{12}\ cm^{-2} \tag{4.8}$$

then

$$I_{rs\ max} \approx 10^{-9}\ amp \quad . \tag{4.9}$$

Since this is the maximum value for the surface recombination current at high forward bias, the contribution that this component makes to the measured current is negligible at all forward bias levels.

Consider the space-charge recombination current by examining Fig. 3.11. At low forward bias the curve labeled (a) in this figure has not only the proper shape, but also the proper order of magnitude to indicate that the excess current seen in the experimental characteristic can be explained as a space-charge recombination current.

For large forward bias, the experimental curve bends away from the linear portion of the curve. This is due to the appearance of an appreciable voltage drop across the spreading resistance region

of the semiconductor at high current levels. The expected series resistance for this diode is

$$R_s = \frac{\rho}{4 r_c} = 28\ \Omega \tag{3.29}$$

The experimental value of R_s is determined with the aid of a digital computer. (For the details of the complete computer program used in this study, the reader is referred to Appendix C.) For a forward applied potential, $V_a \geq 0.4$ volts, the current is described by an expression of the form

$$I_n = I_{no} \exp\left[\frac{q}{kT} (V_a - I_n R_s)\right] \tag{4.10}$$

or

$$\ell n\, I_n - \frac{q V_a}{kT} = \ell n\, I_{no} - \frac{q}{kT} R_s I_n \tag{4.11}$$

Therefore, if $(\ell n\, I_n - q V_a/kT)$ is plotted against I_n, the slope of the curve will be $-(q R_s/kT)$. Using the digital computer to calculate the points for the graph and to do a least-square fit on the points,

$$R_s = 25.9\ \Omega \tag{4.12}$$

Note that the intercept of the curve of Eq. 4.11 is $\ell n\, I_{no}$. The computer program also provides this value.

$$I_{no} = 3.6 \times 10^{-11} \text{ amp} \quad . \tag{4.13}$$

Thus by analyzing the high current, large forward bias portion of the volt-ampere characteristic, a value for saturation current can be found. (This will be extremely important when the effect of stress is considered because in the presence of stress it is very difficult to determine the Schottky linear portion of the volt-ampere characteristic.) The barrier height can now be determined by substituting values for the saturation current, the contact area, Richardson's constant, and the temperature into Eq. 4.1 and solving for the barrier height

$$\varphi_B = 0.807 \text{ ev} \quad . \tag{4.14}$$

This value is in good agreement with the published values for the barrier height of this contact (0.80 ± 0.02 ev)[4-5, 4-6, 4-7, 4-8]. An alternative way of determining the barrier height is to measure the volt-ampere characteristic at different temperatures and determine the saturation current as a function of temperature. Then from Eq. 4.1,

$$\ell n\left(\frac{I_{no}}{T^2}\right) = \ell n(a\,A) - \frac{\varphi_B}{kT} \quad . \tag{4.15}$$

If $\ell n\,[(I_{no})/(T^2)]$ is plotted against $1/kT$, a straight line with slope φ_B should result. The plot of Eq. 4.15 for this diode is shown in

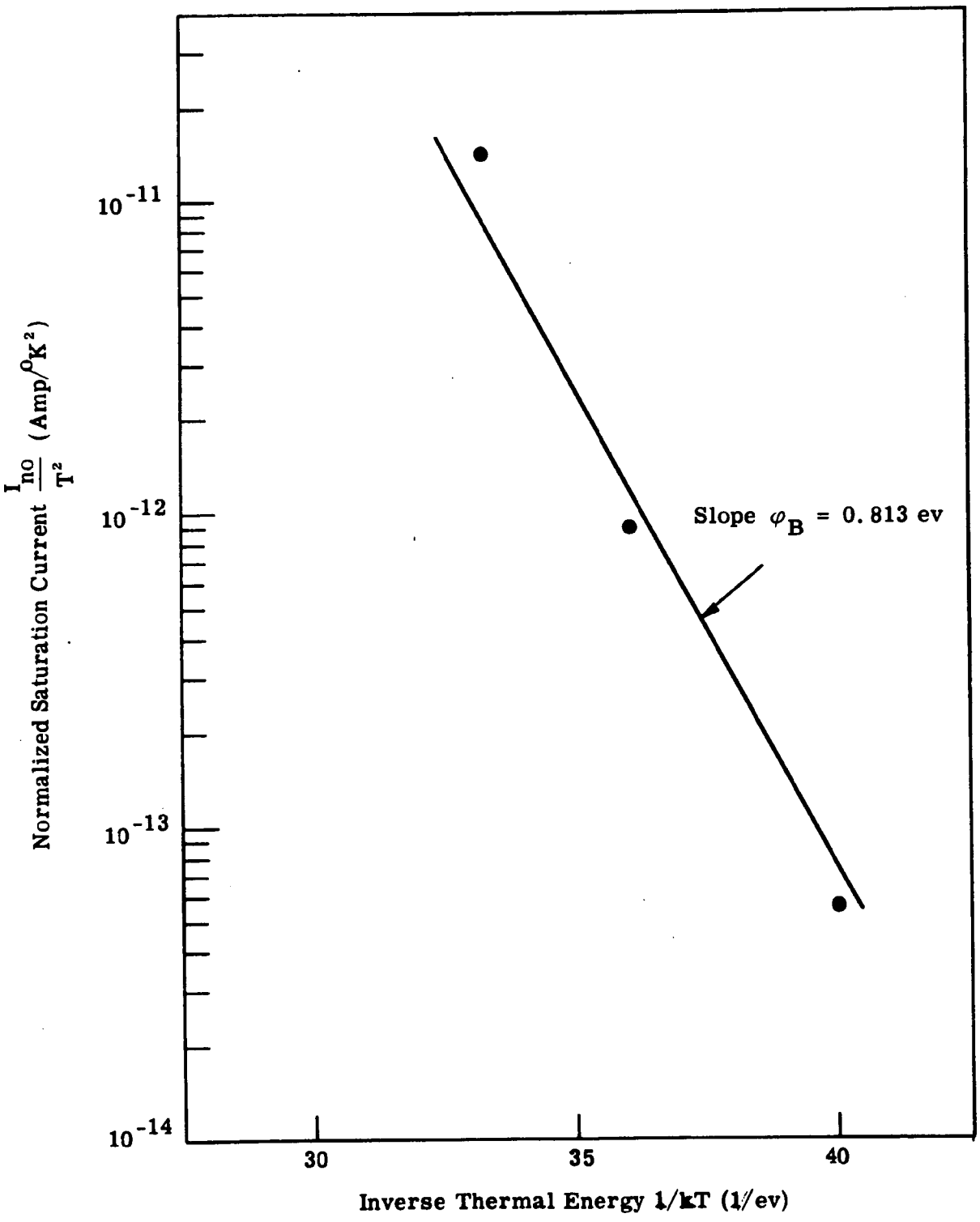


Fig. 4.5 Thermal Activation Energy Plot of the Saturation Current.

Fig. 4. 5. The slope of the curve was determined by a least-square fit to the data. (This is also done on the computer.) Note that the values for the barrier height obtained by the different methods differ by about 1 percent. The barrier heights of six different diodes were determined from thermal activation plots of the saturation current and compared with the barrier heights as determined by substituting values into Eq. 4. 1 and solving for φ_B. The maximum difference between the barrier heights as determined by the two different methods was 5. 2 percent. On the basis of this agreement, the technique of substituting values into Eq. 4. 1 to determine the barrier height is shown to provide sufficient accuracy for this study.

4. 2. 2 Mesa Diodes. The mesa diodes were fabricated as described in Appendix B. A typical mesa diode volt-ampere characteristic is shown in Fig. 4. 6.

The side surface of the mesas is not passivated. [Passivation generally involves the growth of an oxide on the surface. This process reduces the surface recombination velocities and hence the surface leakage currents[4-12].] Therefore, the high reverse current, the large value of η, and the generally poor degree of rectification of this diode is attributed to the presence of large recombination currents.

Considerable effort was put forth in an attempt to improve the quality of the volt-ampere characteristic of the mesa diodes.

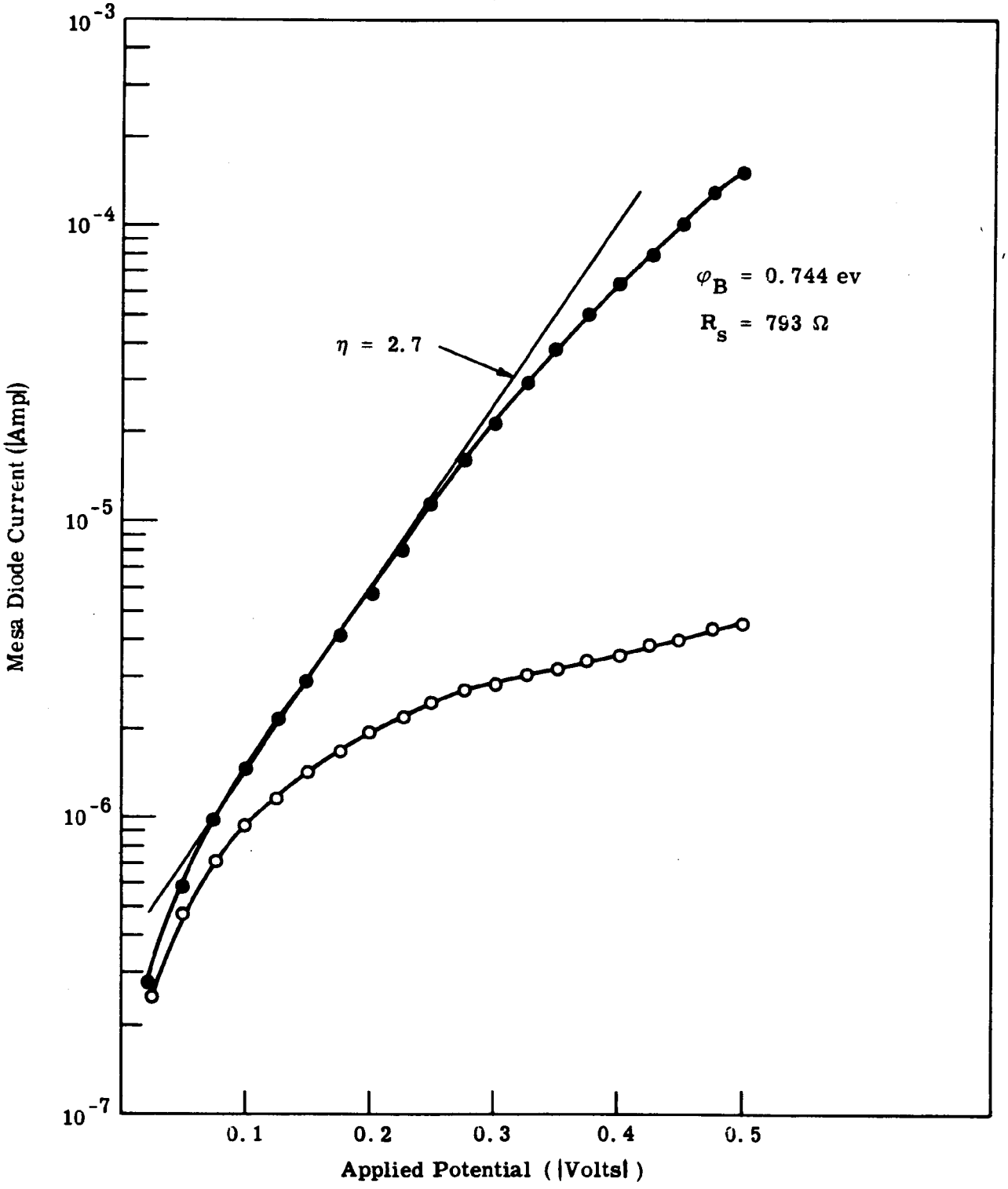


Fig. 4.6 Zero Stress Volt-Ampere Characteristic of Typical Mesa Gold to n-Type Si Contact.

However, the author was finally forced to conclude that the achievement of a high-quality characteristic such as that shown above for a planar diode is beyond his present technological capability.

The relatively high currents for low forward bias and for reverse bias conditions can be treated only by assuming that they are due to high recombination currents. Since some of the quantities involved in the mathematical expressions for the recombination currents cannot be known a priori, it is virtually impossible to determine the relative contributions of the various current components in these voltage regions.

However, in the region of high forward bias, the usual analysis can still be attempted. If these data for $V_a \geq 0.4$ volts are analyzed by means of Eq. 4.11 and Eq. 4.15, the barrier height and series resistance are found to be

$$\varphi_B = 0.774 \text{ ev}$$

and (4.16)

$$R_s = 793\ \Omega$$

The value for the barrier height is close to but slightly smaller than the accepted value. This indicates that for $V_a \geq 0.4$ volts, the majority of the current is probably Schottky current. The value of the series resistance as determined by this technique has the proper order of magnitude when the effect of the constriction of the current

due to the mesa is considered. Therefore, it appears that the high forward bias region can be analyzed with the techniques described above.

4.3 Experimental Volt-Ampere Characteristics with Mechanical Stress

On the basis of the above discussion for the zero stress volt-ampere characteristic of the mesa diode, it appears that data from the mesa diodes can be interpreted only for the effect of stress on the Schottky current. The volt-ampere characteristic of the planar diodes, however, can be useful in determining the effect of stress on both Schottky current and the space-charge recombination current.

4.3.1 Stress Field. In this study, the stress in the space-charge region of the semiconductor is of primary importance. Since the stress is applied by means of a stylus and since both the stylus and the semiconductor have irregular surfaces, the true stress field in the region of interest is highly complex. Therefore some approximate stress field must be assumed.

For the case of the mesa diodes, a stylus with a large radius of curvature [such as that shown in Fig. 4.3(a)] can be used to make contact with the entire gold contact. Because of the mesa configuration, the stress field can be conveniently approximated as a uniaxial field (ignoring the effect of the surface irregularities).

For the case of the planar diodes, one can again ignore surface irregularities and assume the stress field to be that due to a spherical indentor on a semi-infinite plane. This problem has been solved[4-13, 4-14] but unfortunately the resulting stress field is highly anisotropic and nonanalytic. Thus, if an analytic expression for the stress dependent barrier height is desired, an approximation to the stress field must be made. If this is done, maintaining some anisotropic character in the stress pattern, the stress dependent barrier height will be a function of position in the contact area. This results in a nonuniform current density over the contact. Experimentally, only the total current (the integral of the current density over the contact area) can be measured. Thus, any experimentally determined barrier height will be an average, effective barrier for the contact. Thus, from the point of view of the correlation of the experimental data, it is reasonable to assume the stress field for planar diodes to be uniaxial where the magnitude of the stress is determined by dividing the applied force by an effective area.

4.3.2 Effect of Mechanical Stress on Planar Diodes. Figure 4.7 shows the volt-ampere characteristic of a typical planar diode with various amounts of force applied to the contact. The area used to calculate the stress was found by examining the evaporated gold pad under a microscope after the diode had been stressed. The stressed region of the pad is clearly visible (see Fig. 4.8).

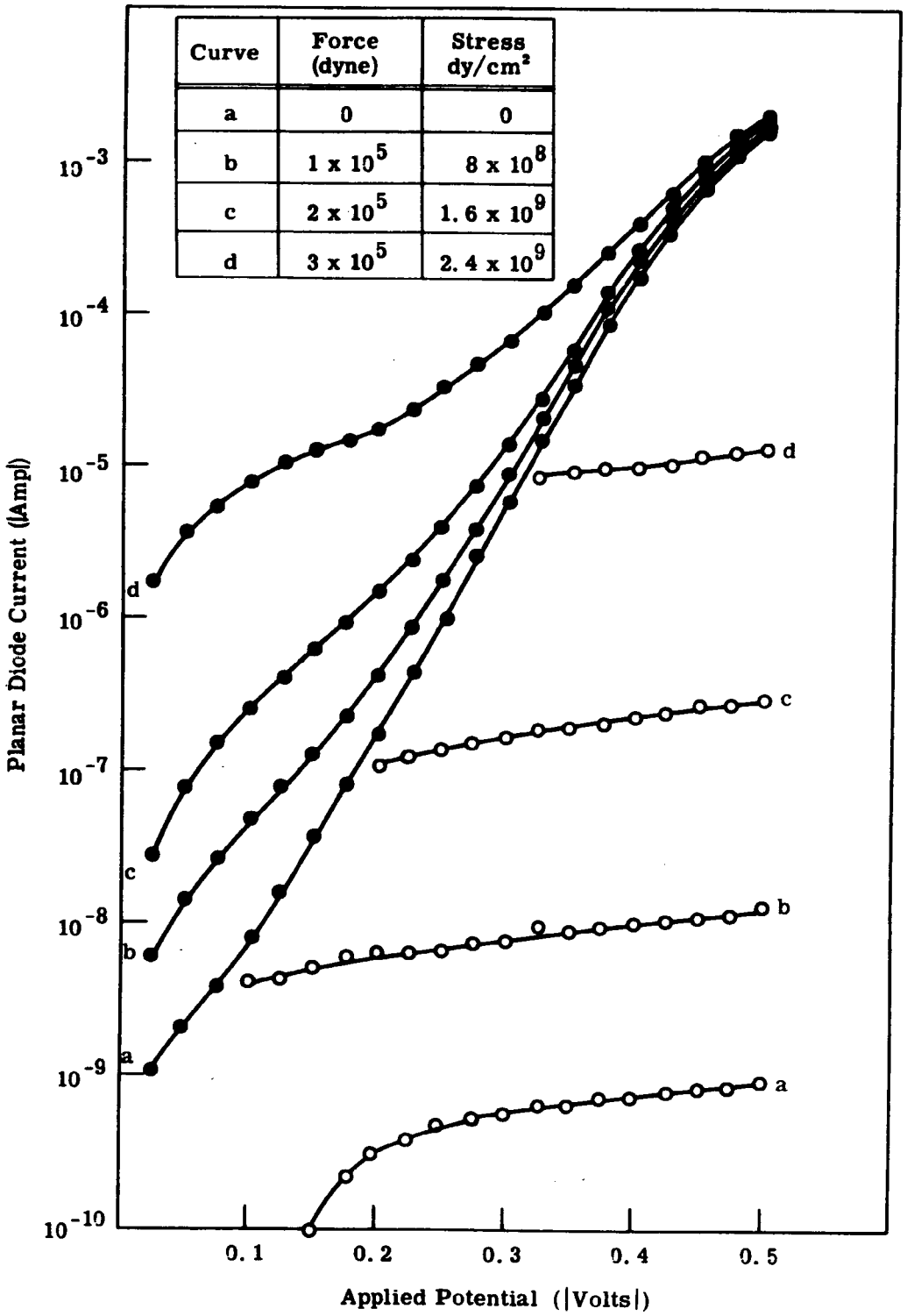


Fig. 4.7 Volt-Ampere Characteristic of Mechanically Stressed Planar Diode.

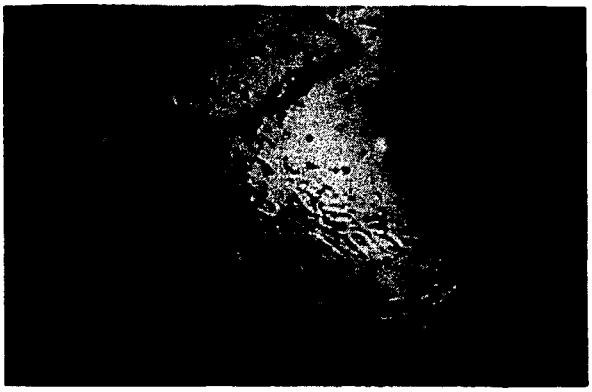


Fig. 4. 8 Photograph of Stressed Gold Contact (400 X).

Examination of the stress dependent characteristic shows a small shift in the high current, large forward bias region and a large shift in the regions of low forward bias and of reverse bias. This suggests large changes in the space-charge recombination current and only small changes in the Schottky current.

The small changes in the Schottky current correlate with the theory since the nominal stresses are relatively small. (Note also that these curves were obtained using the 303 stainless steel stylus which has a yield point of 2.4×10^9 dyne/cm^2.) The stress dependence of the change in the barrier height as determined by the computer analysis of the high current region is shown in Fig. 4.9. Since this curve shows appreciable scatter, it is necessary to consider the average of several diodes in order to verify the prediction given in Chapter III. The stress dependence of the change in the barrier height of seven (3 planar and 4 mesa) diodes is shown in Fig. 4.10. In this figure the ordinate is the change in barrier height times the stressed area. This rather unusual quantity is required because the stressed area is generally different for each of the diodes considered. The theoretically expected dependence is shown by the straight line in the figure. Thus while there is considerable scatter for the data of each diode tested, the average of several diodes has the proper order of magnitude of barrier height stress dependence. Therefore, the prediction of the barrier height stress dependence as given in Chapter III is verified.

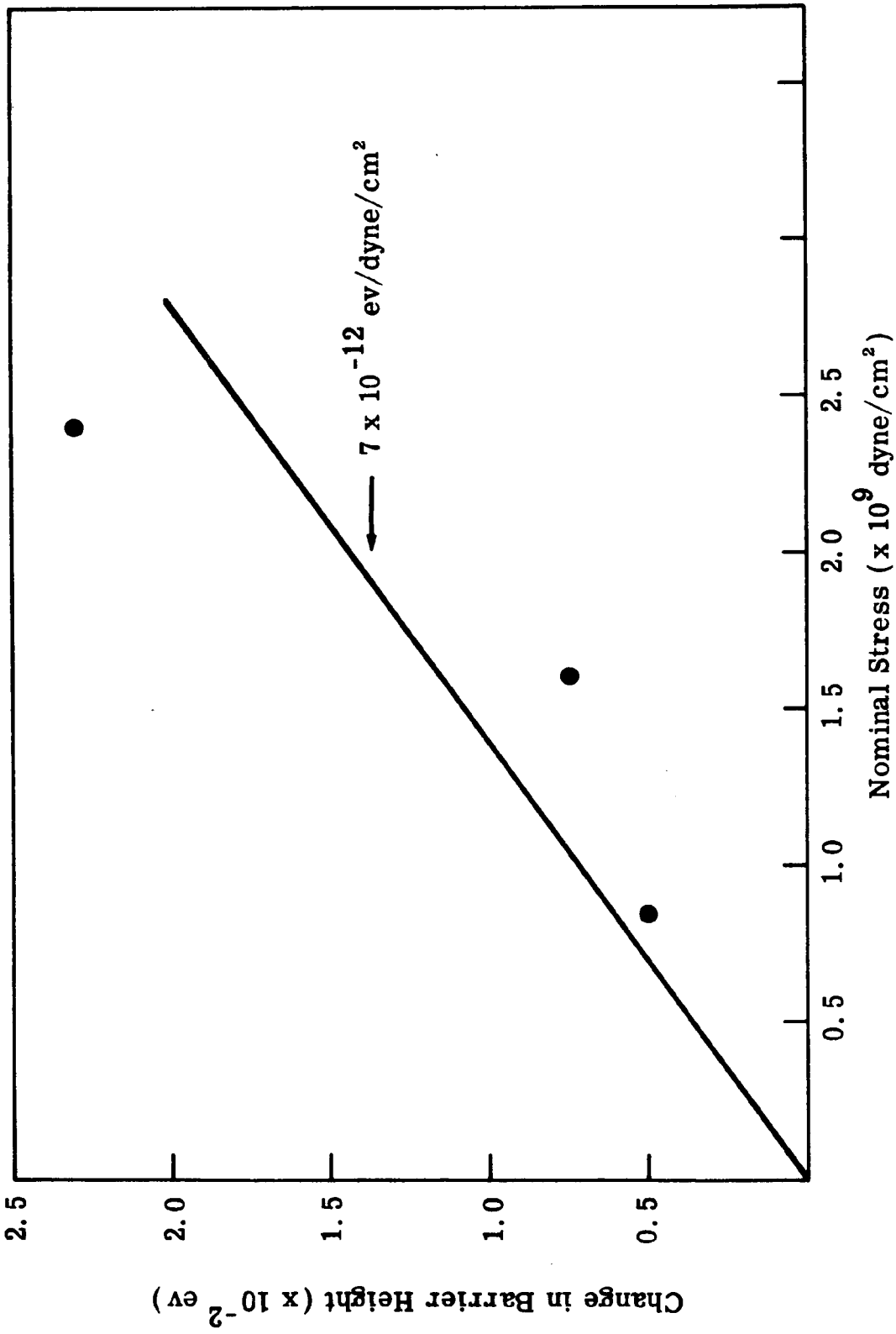


Fig. 4.9 Stress Dependent Change in Barrier Height of Planar Diode.

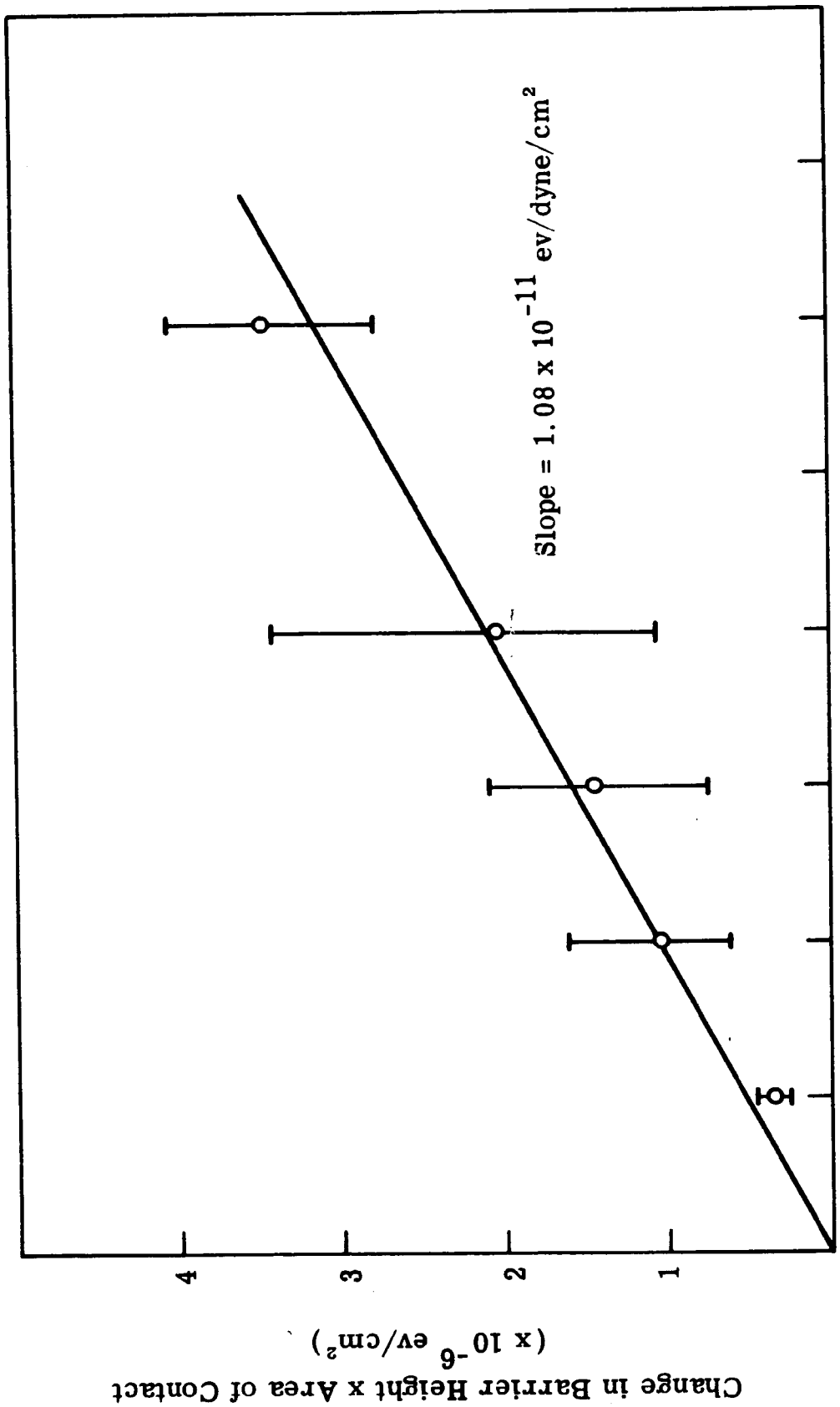


Fig. 4.10 Stress Dependence of Barrier Height (Average of 7 Diodes).

The large shifts in the characteristic at low forward bias and at reverse bias appear to be shifts in the space-charge recombination current component. The stress sensitivity of this current is discussed in Chapter III in terms of two different mechanisms. One, the stress dependence of the density of intrinsic carriers and two, a possible stress dependence of the energy of trapping centers. The first mechanism can be ruled out as the cause for the shift because of the small shift at high current levels. Therefore, it is a shift in the energy of the trapping centers that is indicated. However, caution must be exercised at this point! The energy of trapping centers was not measured; rather a volt-ampere characteristic. It is on the basis of the volt-ampere measurement that a shift of trap energy is suggested.

While no experimental evidence is available to directly verify this suggestion, some evidence is available to support it. It is known[4-15] that some crystalline defects move when a crystal is stressed and then return to their original position when the stress is removed. If the stress is high, some new defects may be introduced. These will remain in the crystal when the stress is removed. Now if a trap level in the forbidden band is associated with a crystalline defect, the physical movement of the defect will result in a change in the trap energy associated with that defect. As long as the defects can relax back to their original positions when the stress is removed, the volt-ampere characteristic will return to the zero stress characteristic

when the stress is removed. However, if the defects are moved so far that they cannot relax to their original position, or if new defects are created when the stress is applied, there will be a permanent shift in the volt-ampere characteristic.

Only a limited amount of data were taken on the reversibility of the stress dependent shifts in the volt-ampere characteristic. However, Fig. 4.11 shows a representative characteristic for a large area (7×10^{-4} cm^2) diode at (a) zero stress, (b) a nominal stress of 2×10^9 dyne/cm^2, and (c) at zero stress again. When the stress is removed, the characteristic remains slightly above its original position. This indicates that the stress caused only a small permanent change in the nature of the contact. This may be explained on the basis of the rather tenuous crystalline defect argument presented above.

It is interesting to note that this also correlates with something that Rindner[4-16] and Diamond[4-17] have observed. Both have noticed that after an initially high stress is applied to a p-n junction (Rindner) or metal-semiconductor point contact (Diamond), the stress sensitivity with smaller stresses is improved. It may be that the initial application of a high stress generates a large number of permanent traps. The subsequent application of smaller stresses may then shift the effective energy of these traps as described above.

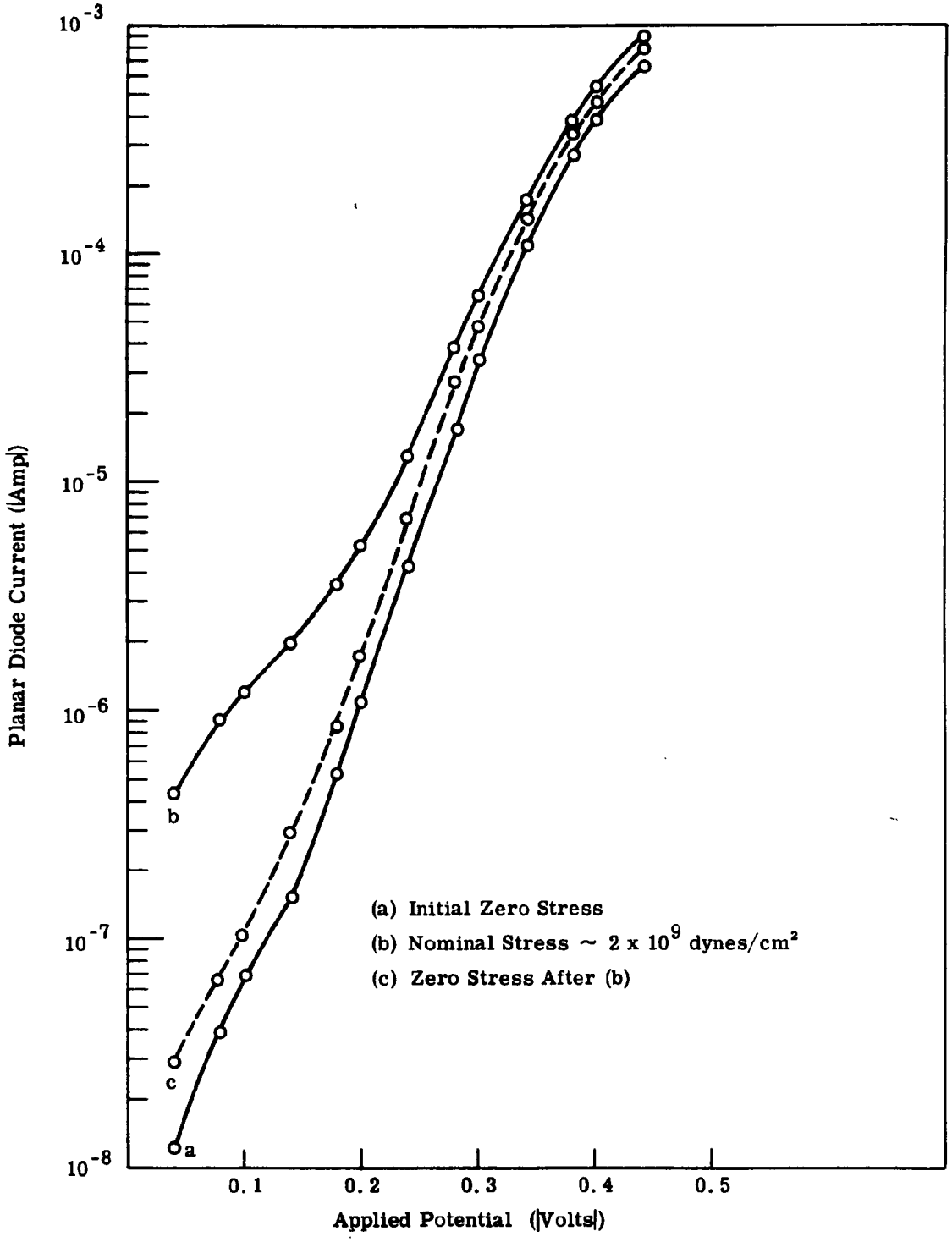


Fig. 4.11 Forward Volt-Ampere Characteristic.

4.4 Summary

In this chapter the experimental procedure used in this study is described. The experimental, zero stress, volt-ampere characteristic for an evaporated gold contact on n-type silicon is explained as expected from a Schottky Barrier diode which has an observable space-charge recombination current component. The stress dependence of the observed barrier height is shown to be essentially that predicted in Chapter III. The large, stress induced, increase in the observed current in the low forward bias and reverse bias regions is explained as an increase in the space-charge recombination current component. The increase in this component can be explained by assuming that the trap energy moves toward the intrinsic energy as the device is stressed.

CHAPTER V

SUMMARY AND CONCLUSIONS

The equations for the various current components of a rectifying metal-semiconductor contact have been developed using the Schottky theory and an analogy to the p-n junction. The zero stress volt-ampere characteristic of a vacuum evaporated gold contact on n-type silicon has been explained on the basis of these equations. The current in the high forward bias region ($V_a \geqq 0.2$ volts) is shown to be a Schottky current of electrons over a potential energy barrier, φ_B. The current in the low forward bias region and in the reverse region (-0.5 volts $\leqq V_a \leqq +0.2$ volts) is explained by the presence of a space-charge recombination current component.

When a compressive mechanical stress is applied to the contact, the volt-ampere characteristic shifts in the direction of a decreasing contact resistance. An energy band shifting theory proposed by Wortman[5-1] is extended to predict the mechanical stress dependence of the contact barrier height. This allows a determination of the effect of mechanical stress on the Schottky current. This prediction is verified by the experimental data.

For an applied stress such that there is only a small change in the Schottky current (i.e., $\sigma < 3 \times 10^9$ dyne/cm^2), the volt-ampere

characteristic of the contact shifts by a large amount in the applied potential range from -0.5 volts to +0.2 volts. In this voltage range, the stress-dependent recombination current changes more rapidly than can be accounted for solely on the basis of the band shifting theory. Since some of the quantities which appear in the expressions for the recombination current components are difficult to determine, it is impossible to present a detailed theory of the stress dependence of these currents. However, a discussion is presented of how a stress dependent change in the energy of generation-recombination centers might arise. This leads to an expected change in the space-charge recombination current that correlates with the experimental data presented in this report. Moreover, this model offers an explanation for the fact that a device sometimes requires the application of a high initial stress before it becomes highly stress sensitive.

Therefore, two conclusions can be drawn from this investigation. One, the extension of Wortman's[5-1] band shifting theory for p-n junctions to the case of the rectifying metal-semiconductor contact yields an accurate prediction of the stress dependence of the barrier height of the contact. Two, another more significant effect appears to be the stress dependent shift in the trap energy relative to the intrinsic energy.

APPENDIX A

STRESS STRAIN RELATIONS

In Chapter III various notations are used to denote the stress and strain in the semiconductor. A brief review of this notation is presented in this appendix. For a more complete treatment the reader is referred to References A-1 and A-2. For crystals with cubic symmetry, a set of orthogonal axes, x, y, z, can be defined to coincide with the (100), (010) and (001) crystalline directions respectively. The stress can be expressed as:

$\sigma_{\alpha\beta}$ = conventional stress, where α, β = x, y, z

σ_{ij} = tensor stress, where i, j = 1, 2, 3

σ_{r} = engineering stress, where r = 1, 2, 3, 4, 5, 6

and where $\sigma_{\alpha\beta} = \sigma_{\beta\alpha}$ and $\sigma_{ij} = \sigma_{ji}$. The various notational forms are related as shown below.

Principle Stress	Shear Stress
$\sigma_{xx} = \sigma_{11} = \sigma_{1}$	$\sigma_{xy} = \sigma_{12} = \sigma_{4}$
$\sigma_{yy} = \sigma_{22} = \sigma_{2}$	$\sigma_{xz} = \sigma_{13} = \sigma_{5}$
$\sigma_{zz} = \sigma_{33} = \sigma_{3}$	$\sigma_{yz} = \sigma_{23} = \sigma_{6}$

The various components of strain can be expressed similarly.

$e_{\alpha\beta}$ = conventional strain, where α, β = x, y, z

e_{ij} = tensor strain, where i, j = 1, 2, 3

e_r = engineering strain, where r = 1, 2, 3, 4, 5, 6

and where $e_{\alpha\beta} = e_{\beta\alpha}$ and $e_{ij} = e_{ji}$. Again the various notations are related as:

Principle Strain	Shear Strain
$e_{xx} = e_{11} = e_1$	$e_{xy} = e_{12} = e_4$
$e_{yy} = e_{22} = e_2$	$e_{xz} = e_{13} = e_5$
$e_{zz} = e_{33} = e_3$	$e_{yz} = e_{23} = e_6$

For a crystal with cubic symmetry the stress and strain are related by Hooke's law which has the form:

$$\begin{bmatrix} \sigma_1 \\ \sigma_2 \\ \sigma_3 \\ \sigma_4 \\ \sigma_5 \\ \sigma_6 \end{bmatrix} = \begin{bmatrix} c_{11} & c_{12} & c_{12} & 0 & 0 & 0 \\ c_{12} & c_{11} & c_{12} & 0 & 0 & 0 \\ c_{12} & c_{12} & c_{11} & 0 & 0 & 0 \\ 0 & 0 & 0 & c_{44} & 0 & 0 \\ 0 & 0 & 0 & 0 & c_{44} & 0 \\ 0 & 0 & 0 & 0 & 0 & c_{44} \end{bmatrix} \cdot \begin{bmatrix} e_1 \\ e_2 \\ e_3 \\ e_4 \\ e_5 \\ e_6 \end{bmatrix}$$

and

$$\begin{bmatrix} e_1 \\ e_2 \\ e_3 \\ e_4 \\ e_5 \\ e_6 \end{bmatrix} = \begin{bmatrix} s_{11} & s_{12} & s_{12} & 0 & 0 & 0 \\ s_{12} & s_{11} & s_{12} & 0 & 0 & 0 \\ s_{12} & s_{12} & s_{11} & 0 & 0 & 0 \\ 0 & 0 & 0 & s_{44} & 0 & 0 \\ 0 & 0 & 0 & 0 & s_{44} & 0 \\ 0 & 0 & 0 & 0 & 0 & s_{44} \end{bmatrix} \cdot \begin{bmatrix} \sigma_1 \\ \sigma_2 \\ \sigma_3 \\ \sigma_4 \\ \sigma_5 \\ \sigma_6 \end{bmatrix}$$

where the c's are called the elastic stiffness constants or moduli of elasticity and the s's are called the elastic constants or the elastic compliance constants.

For pure silicon at room temperature[A-3]

$c_{11} = 1.657\ (10^{12}\ \text{dyne/cm}^2)$ $\qquad$ $s_{11} = 0.768\ (10^{-12}\ \text{cm}^2/\text{dyne})$

$c_{12} = 0.639$ $\qquad$ $s_{12} = -0.214$

$c_{44} = 0.796$ $\qquad$ $s_{44} = 1.257$

If for some reason it is not convenient to use a coordinate system coincident with the lattice cube edges, the usual coordinate transformations can be performed. (See, for example, References A-4 and A-5.)

APPENDIX B

FABRICATION OF EVAPORATED Au-n TYPE Si CONTACTS

This appendix contains as many of the details of the fabrication process as the author is able to present. It is included since the majority of the readers (The University of Michigan, Microelectronics staff) are unfamiliar with the techniques used.

The fabrication of an evaporated contact diode, ready for testing, can be divided into three general areas:

1. The preparation of the semiconductor
2. The evaporation of the metal
3. The attachment of leads

Each of these areas is presented below in a "cookbook" manner.

1. Preparation of the Silicon

It is assumed that the silicon is initially in the form of wafers and that the surfaces of the wafers have a surface finish on the order of 30 μ (i.e., lapped surfaces).

A. Polishing

Polishing of the silicon wafer is done on a polishing wheel rotating at about 250 r.p.m. The wheel is covered with Buehler Ltds., Evanston, Illinois

AB TEXMET cloth. The wafer is mounted to a cylindrical metal slug with Aprezon W ("black wax"). The slug is then placed on a holder which is attached to an oscillator arm (approx. 4 sec. period). See Fig. B. 1. When the oscillator arm is moved across the center of the polishing wheel, the slug in the holder is spun so that the wafer can be uniformly mechanically polished. Lindy A (0.3 μ average grit size, Al_2O_3) abrasive is used with distilled water.

Procedure:

1) Heat the slug on a hot plate (approx. 90°C) and apply a coating of black wax.
2) Place the wafer on the hot, coated slug. Use a cotton bud to work the wafer into the wax coating.
3) Remove the slug from the hot plate and let cool slowly. (An inconclusive amount of experience on the part of the author suggests dislocations can be introduced in Si from a rapid quench, e.g., into H_2O, from a temperature of approximately 150°C. This is surprising since the literature[B-1] indicates that the quench rate of Si from temperatures below 400°C is not important.)

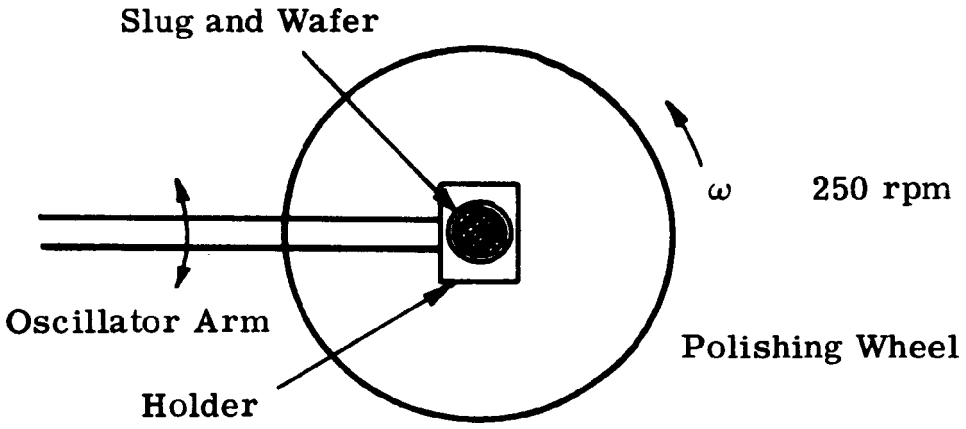


Fig. B. 1 Mechanical Polishing Arrangement.

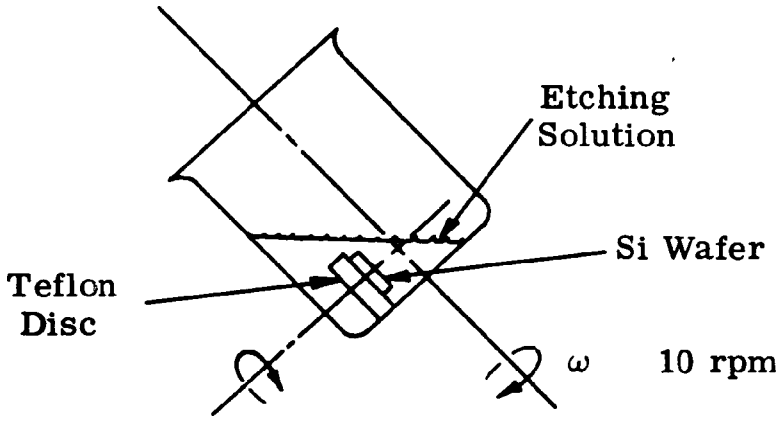


Fig. B. 2 Rotary Etching Arrangement.

4) Start polishing wheel and wet with distilled water.

5) Mount cooled slug in holder and start oscillator.

6) Using a salt shaker, apply Lindy A abrasive.

7) Apply water and abrasive at approximately 45-minute intervals for 3 hours.

8) Let wafer polish for approximately 1 hour after last application of water and abrasive.

The pressure on the wafer should be approximately 1/2 p. s. i. during this polishing cycle. A mirror-finish surface will result.

The wafer now has a smooth surface. However, this surface still contains work damage which may extend several microns into the wafer. In order to remove this damage, chemical polishing (etching) is used.

B. Etching

When Si wafers are etched, the etched surface is generally roughened ("orange peel" effect). While there are techniques, such as using HCL at elevated temperatures, that minimize the orange peel, the most typical echant is a Nitric-Hydrofloric-Acetic combination (CP4-A). In an effort to make the etching as uniform as possible, rotary etching schemes have been developed. See Fig. B. 2.

Procedure: Cleaning Prior to Etch

1) Heat the polishing slug until the wax softens. Slide the wafer off the slug and place on filter paper to cool.
2) Rinse the wafer in trichloroethyene (TCE) until all excess black wax is removed.
3) Ultrasonically clean wafer in clean beaker with reagent grade TCE for 5 minutes.
4) Change TCE and ultrasonically clean for 5 minutes.
5) Change TCE and ultrasonically clean for 5 minutes.
6) Remove wafer and store in clean beaker with fresh TCE.

ii Procedure: Etching

1) Clean Etching beaker and Teflon disk.
2) Place 3 parts of 49% HF, 3 parts Glacial Acetic acid and 16 drops of Br/50cc of final etch into the rotating etching beaker.
3) While the above is mixing, mount the Si wafer on the Teflon disk with black wax.
4) After disc has cooled, insert it into the beaker.
5) Wait 2 minutes.
6) Add 5 parts 70% HNO_3.

7) Wait 2 minutes. The etching rate is approximately 0.5 μ/min.

8) Quench the etching by adding as much distilled H_2O as possible.

9) Remove beaker from rotating arm and rinse thoroughly with distilled H_2O.

10) Remove wafer from disc and clean as described in B-i above.

C. n+ Diffusion

An n+ diffusion is performed in order to prepare an ohmic contact to the bottom (lapped surface) side of the wafer.

Procedure:

1) Remove the wafer from the TCE.

2) Dry the wafer using an IR lamp or hot plate.

3) Immerse the wafer in a 1:1 solution of 49% HF to distilled water for about 1 minute.

4) Rinse thoroughly with distilled H_2O.

5) Dry the wafer as in Step 3.

6) Place the wafer on the diffusion boat.

7) Insert boat into diffusion tube up to the edge of the furnace.

8) Wait 5 minutes —check furnace: 1200^{o}C with dry Argon flowing.

9) Move boat to center of diffusion tube.

10) Add 18cc/min. dry O_2.

11) Gradually add 2.1 s.c.f.h. of 1000 p.p.m. PH_3 — carrier gas Argon (Phosphine). At the same time gradually decrease the A flow to zero.

12) Wait 30 minutes. This yields an n+ layer approximately 3 μ deep.

13) Shut off PH_3 and O_2; turn on A to flush the tube.

14) Wait 5 minutes.

15) Move diffusion boat to edge of furnace.

16) Wait 15 minutes.

17) Remove boat from diffusion tube and let wafer and boat cool together.

D. Post Diffusion Etching

The wafer now has an n+ region on all sides. The n+ region has to be removed from the top side. If the boat and wafer are placed in a laminar flow bench to cool, no cleaning procedure is required prior to etching.

Procedure:

1)-7) Repeat the steps described in Section B-ii above.

8) Quench the etching by adding as much 70% HNO_3 as possible.

9) Rinse with 70% HNO_3.

10) Store the wafer on the Teflon disc in HNO_3 until ready to proceed with the oxidation step.

E. Oxidation

The purpose of oxidizing the freshly etched top surface of the wafer is to put a protective coating over this surface. The HNO_3 quench in the above step is to form a thin oxide coating (approx. 50 $\mathring{A}$). This thin oxide layer helps to keep the Si surface free from contamination during the cleaning step prior to oxidation in the furnace.

Only a few hundred angstroms (approx. 300 $\mathring{A}$) of oxide is grown in the furnace. This is thick enough to protect the Si surface from absorbing impurities and thin enough to avoid problems due to the "snow plow" effect. When an oxide is grown on a phosphorous-doped silicon wafer, the phosphorus atoms do not go into the oxide, but are pushed back into the bulk Si. This is called the "snow plow" effect. The result of this effect is to introduce a high density of phosphorus donor atoms into the space-charge region. This high densityof positive charge reduces the barrier width thus causing a significant reduction in the effective barrier height.

Procedure:

1) Establish a furnace temperature of 800°C with an Argon atmosphere.
2) Mount the clean wafer on the oxidation boat and insert into the center of the oxidation tube.
3) Turn off the Argon.
4) Turn on 150cc/min. dry O_2.
5) Wait 30 minutes.
6) Turn off O_2 and turn on A.
7) Wait 5 minutes.
8) Remove oxidation boat and wafer and let cool together.

F. Evaporation and Drive in of Base Contact

The lapped side of the wafer (the bottom side) now has an n+ layer covered by a few hundred angstroms of oxide. To insure good contact between this n+ layer and the header, the procedure described below is used.

Procedure:

1) Black wax the top of the wafer.
2) Immerse the wafer in 49% HF.
3) Wait about 30 seconds.

4) Remove the wafer from the HF and place into the vacuum chamber—bottom side toward A source.
5) Pump down vacuum chamber and deposit from 1500 A to 2000 A of Au. (Evaporation conditions not critical.)
6) Remove wafer from vacuum chamber and clean wafer in TCE.
7) Establish a furnace temperature of 500^{o}C with an Argon atmosphere. (Note eutectic temperature for Au-Si is 350^{o}C.)
8) Place the wafer on the boat and slide the boat into the center of the furnace.
9) Wait about 1 minute.
10) Remove boat and check for partial Au drive in. Repeat Steps 8 and 9 if necessary.
11) Let wafer and boat cool together.

G. Evaporation of Rectifying Contacts

Two cm of 13-gauge Au wire (99.999%) from Gallard Schlesinger Chemical Mfg. Corp. is evaporated from a W helix 15 cm from the substrate. The source is shuttered to prevent contaminates being evaporated onto the Si. The evaporation is done through a molybdenum

mask. The mask has a 1-square inch array of 0.005 inch diameter holes on 0.020 inch centers. Also in the array are three 0.0135 inch diameter holes. These large area contacts are used for alignment patterns in the photo-resist process described below. The Si wafer is heated during the evaporation. Si temperatures from 150°C to 200°C have been used with no observable variation in V-I characteristic. Liquid nitrogen is always used in the baffle to reduce any back-streaming that may be present.

Procedure:

1) Thoroughly clean 2 cm of 13-gauge Au wire and insert into the W helix.
2) Establish the desired temperature of the substrate heater.
3) Clean the Si wafer in TCE and dry with IR lamp.
4) Immerse the wafer in 49% HF for about 1 minute.
5) Remove the wafer from the HF and blot the excess HF off the Au coated bottom side. Note HF will not wet a clean Si surface. Thus any HF droplets remaining on the top side of the wafer indicates incomplete oxide removal and/or contamination of the top surface.

6) Place the wafer on the substrates heater in the vacuum chamber.

7) Place the moly mask over the wafer.

8) Close the shutter and evacuate the bell jar.

9) Establish a vacuum of at least 1×10^{-6} torr.

10) Adjust substrate temperature to desired temperature.

11) Heat W helix until Au wire wets the helix.

12) Open shutter and evaporate all of the Au charge. A conductivity slide monitor is used to insure a sufficiently thick coating of Au i.e., about 1500 A. The conductivity of Au films is 1.71 Ω/□/1000 A. This conductivity calibration was done with a Talansky multiple beam interferometer and films thickness between 1000 A and 3000 A.

13) Remove the wafer from the vacuum station.

H. Photo-Resist Procedure for Mesa Diodes

If mesa diodes are desired the procedure below can be used. However, the reader is forewarned that the yield will be very low (~ 5%) when the contact diameter is on the order of 0.005 inch.

The etching appears to be the crucial step. The author has tried a variety of etchants and etching

procedures—all with only slight success. The procedure below worked the best of all those tried, however, the author is confident that a better technique must exist.

Procedure:

1) Clean the wafer in TCE.
2) Dry with an IR lamp.
3) Place the wafer on the whirl coater and place 5 drops of 1:1 Kodak Metal Etch Resist (KMER) to KMER thinner on the wafer. Note the KMER should be centrifuged and the lighter 1/2 used.
4) Whirl coat at 250 r.p.m. for a few seconds.
5) Prebake the coated wafer on a hot plate at $80^{o}C$ for 15 minutes. (A vacuum furnace would be better.)
6) Optically align the evaporation mask over the wafer.
7) Expose the photo-resist for 20 seconds with a high intensity Hg source.
8) Immerse exposed wafer in KMER developer for 2 minutes.
9) Remove the wafer from the developer and dip it into a small beaker of Xylene.
10) Rinse under about $35^{o}C$ running tap water.

11) Examine photo-resist pattern—check for proper development.

12) Postbake the wafer on a hot plate at 110°C for 30 minutes. (Again a vacuum furnace would be better.)

ii Procedure: Mesa Etch

1) Coat the bottom side of the wafer with black wax.

2) Prepare a solution of CP4:

3 HF
3 H Ac
5 HNO_3
16 drop Br/50cc

3) Place 50cc of this etch in a 600 ml poly beaker.

4) Immerse the wafer in the etch.

5) Wait 10 seconds.

6) Quench with HNO_3. This forms a partial oxide passivation on the mesa edge.

7) Rinse thoroughly with distilled H_2O.

8) Remove black wax with TCE.

iii Procedure: Resist Removal

1) Use J-100, a photo-resist stripper manufactured by Indust-RI-Chem Laboratory, Richardson, Texas.

2) Place 50cc of J-100 in clean beaker and heat to about 95°C.

3) Immerse wafer.

4) Wait 2 minutes.

5) Remove wafer and rinse in TCE.

6) Dry wafer and check optically for resist removal.

7) Repeat process if necessary.

I. Scribing and Mounting of Dice

While it is possible to mount an entire wafer on a header, note that a chip 0.1-square inch has 25 diodes on it. Therefore, in most instances it is more convenient to scribe the wafer into dice on the order of 0.1 inch on a side. The solder used in the mounting procedure is Indalloy No. 8 with Indalloy flux No. 2, supplied by Indrum Corporation of America, Utica, New York. This solder has a low temperature melting point (~ 90°C) and wets well to brass and to gold.

Procedure: Scribing

1) Place the wafer bottom side down on a firm surface.

2) Using a straight edge (e.g., a microscope slide) and a diamond scribe, scribe the cross hatch pattern on the top surface of the wafer. Use a firm even stroke.

3) Place the scribed wafer between two pieces of paper.

4) Align one set of scribe lines parallel with the edge of a desk or bench.

5) Grasp the paper firmly and roll the wafer over the edge.

6) Rotate the wafer 90^{o} and roll over the edge again.

7) Examine the disc and repeat process for those that have failed to break.

ii Procedure: Mounting Dice onto Brass Header

1) Tin the Au coated bottom side of the wafer. Use a fine tip, low temperature soldering pencil.

2) Using a hot plate, tin the brass header.

3) Sweat the chip onto the header. Use the minimum amount of heat. (Remember the eutetic temperature of Au-Si is $350^{o}C$.)

APPENDIX C

DATA ANALYSIS COMPUTER PROGRAM

Since a large part of the data analysis was done on the digital computer, a detailed explanation of the program is presented here.

The computer program was written in MAD and will accept, as input data, the current measured at 25 millivolt intervals over the range from -0.5 volts to +0.5 volts applied potential. Nine different forces and five different temperatures (i.e., 45 sets of volt-ampere data) can be accepted in a single data run. The first operation is done by considering the forward characteristic for $V_a \geq 0.4$ volts. The points necessary for a plot of Eq. 4.11 are computed.

$$\ell n\, I_n - \frac{q V_a}{kT} = \ell n\, I_{no} - \frac{q R_s}{kT} I_n \qquad (4.11)$$

A straight line is then fit by least-squares to the points and the slope (R_s) and the intercept ($\ell n\, I_{no}$) are determined. The value of I_{no} is then determined and that together with the theoretical value for Richardson's constant and the input data for the contact area and the temperature are used to compute the barrier height (see Eq. 4.1)

$$\varphi_B(F, T) = kT\, \ell n\left(\frac{a A T^2}{I_{no}}\right) \qquad (C.1)$$

As indicated in Eq. C. 1, this is done for each different force and temperature.

If more than two different temperatures are used, the points necessary for a plot of the thermal activation of the saturation current are computed.

$$\ell n\left(\frac{I_{no}}{T^2}\right) = \ell n(a\,A) - \frac{\varphi_B}{kT} \qquad (4.15)$$

A straight line is fit by least-squares to the data and the slope (φ_B) and the intercept ($\ell n\, a\, A$) are determined.

An additional feature of the program, not mentioned in the text of this report, is the capability to compute the theoretical Schottky characteristic on the basis of the experimentally determined values for the barrier height and the series resistance of the contact. The difference between this theoretical Schottky current and the measured current can then be computed.

It is also possible to consider the measured characteristic as being two diodes in parallel, one stress dependent and the other independent of stress. The division of the measured current is done by considering only part of the total evaporated contact area as being the area over which the stress is applied. The current through the unstressed area is assumed to be constant and is subtracted from each of the stress dependent characteristics. The resulting data for the stress sensitive part of the diode is then reanalyzed as if it were the

original input data. It was the author's experience that this type of analysis does not yield any more information. Therefore, the results of this extended analysis were not used.

The complete program listing is shown below:

```
$COMPILE MAD, EXECUTE, PRINT OBJECT, I/O DUMP

MAD (02 NOV 1966 VERSION) PROGRAM LISTING ... ... ...


            REFERENCES ON
            INTEGER I,J,K,M,N,START,STOP,P
            DIMENSION T(5),F(9),VA(40),ID(9*5*40), Y(9*5*40), YY(9*5),
           1 SX(9*5),SY(9*5),SXY(9*5),SX2(9*5),RS(9*5),LNIO(9*5),XX(9),
           2       SYY(9),SYYXX(9),PHIB(5),AAA(5) ,X(9*5*40),IO(9*5)  ,
           3  CONST(5)  , PHIIO(9*5), EXRC(5), IT(9*5*40), IEX(9*5*40)
            DIMENSION SI(9*5*40)
            VECTOR VALUES PI = 3.1415
            VECTOR VALUES Q=1.6E-19
            VECTOR VALUES KK = 8.63 E-5
            VECTOR VALUES E = 1.06 E -12
            VECTOR VALUES RC = 120
            VECTOR VALUES VA(1) = .025, .05, .075, .1, .125, .15, .175, .2
           1 .25, .275, .3, .325, .35, .375, .4, .425, .45, .475, .5,
           2  .025, .05, .075, .1, .125, .15, .175, .2, .225, .25, .275,
           3  .3, .325, .35, .375, .4, .425, .45, .475, .5
     XXX    PRINT COMMENT $1THERMAL- STRESSED DIODE ANALYSIS $
            READ AND PRINT DATA
     YYY    START = 17
            STOP = 20
            THROUGH AA, FOR I = 1,1,I.G.M
            THROUGH AA, FOR J = 1,1, J.G.N
            THROUGH AA, FOR K = START,1,K.G.STOP
            Y(I,J,K) = ELOG.(ID(I,J,K))-(  VA(K))/(KK*T(J))
      AA    X(I,J,K) = (-  ID(I,J,K))/(KK*T(J))
            PRINT COMMENT$1LEAST SQUARE FIT FOR RS(I,J) AND LNIO(I,J)
            THROUGH AA1, FOR I=1,1, I.G.M
            THROUGH AA1, FOR J=1,1, J.G.N
            SX(I,J) = 0
            SY(I,J) = 0
            SXY(I,J) = 0
     AA1    SX2 (I,J) = 0
            THROUGH AA2, FOR I = 1,1, I.G.M
            THROUGH AA2, FOR J =1,1, J.G.N
            THROUGH AA2, FOR K = START,1,K.G.STOP
            SX(I,J) = SX(I,J) + X(I,J,K)
            SY(I,J) = SY(I,J) + Y(I,J,K)
            SXY(I,J) = SXY(I,J) + X(I,J,K)*Y(I,J,K)
     AA2    SX2(I,J) = SX2(I,J) + Y(I,J,K).P.2
            THROUGH CC, FOR I=1,1,I.G.M
            THROUGH CC , FOR J=1,1,J.G.N
            RS(I,J)=((STOP-START+1)*SXY(I,J)-SX(I,J)*SY(I,J))/((STOP-
           1 START       +1)*SX2(I,J)-SX(I,J).P.2)
            LNIO(I,J)=(SY(I,J)*SX2(I,J)-SX(I,J)*SXY(I,J))/((STOP-START+1)
           1 *SX2(I,J)-SX(I,J).P.2)
            IO(I,J) = EXP.(LNIO(I,J))
            PHIIO(I,J)= -KK*T(J)*(LNIO(I,J)-ELOG.(.785*DT*DT*PC*T(J)*
      V    1 T(J)))
      CC    PRINT RESULTS F(I), T(J), PHIIO(I,J), RS(I,J), IO(I,J)
            WHENEVER N .L. 2, TRANSFER TO AAB
            THROUGH DD , FOR J =1,1, J.G.N
     DD     XX(J) = 1./(KK*T(J) )
            THROUGH EE, FOR I=1,1, I.G.M
```

```
          THROUGH EE, FOR J=1,1,J.G.N
EE        YY(I,J) = LNIO(I,J)-2*ELOG.(T(J))
          PRINT COMMENT $1LEAST SQUARE FIT FOR PHIB(I) AND AAA(I) $
          SXX2 = 0
          SXX = 0
          THROUGH FF, FOR I=1,1, I.G.N
          SXX = SXX + XX(I)
FF        SXX2 = SXX2 + XX(I).P.2
          THROUGH GG , FOR I = 1,1, I.G.M
          SYY(I) = 0
GG        SYYXX(I) = 0
          THROUGH HH, FOR I =1,1, I.G.M
          THROUGH HH, FOR J =1,1, J.G.N
          SYY(I) = SYY(I) + YY(I,J)
HH        SYYXX(I)=SYYXX(I) + YY(I,J)*XX(J)
          THROUGH II, FOR I=1,1, I.G.M
          PHIB(I)=(N*SYYXX(I)-SXX*SYY(I))/(N*SXX2-SXX.P.2) *(-1.)
          AAA(I)=(SYY(I)*SXX2-SXX*SYYXX(I))/(N*SXX2-SXX.P.2)
          CONST(I) = EXP.(AAA(I))
          EXRC = CONST(I) / (.785*DT*DT)
II        PRINT RESULTS F(I), PHIB(I), AAA(I), CONST(I) , EXRC
AAB       THROUGH AB, FOR I =1,1, I.G.M
          THROUGH AB,FOR J = 1,1, J.G. N
          THROUGH AB , FOR K = 1,1, K.G. 40
AB        IT(I,J,K) =IO(I,J)*(EXP.((1/(KK*T(J)))*VA(K))-1)
          THROUGH AC, FOR I = 1,1, I.G. M
          THROUGH AC, FOR J = 1,1, J.G. N
          THROUGH AC , FOR K = 1,1, K.G. 16
          THROUGH AE, FOR P=1,1, P.G.20
          FUNC = IT(I,J,K) - IO(I,J)*(EXP.((1/(KK*T(J)))*(VA(K)-
        1 IT(I,J,K)*RS(I,J))) - 1)
          FUNCP = 1 + (RS(I,J)*IO(I,J)/(KK*T(J)))*EXP.((1/(KK*T(J)))*
        1 (VA(K)- IT(I,J,K)*RS(I,J)))
          ITT = IT(I,J,K) - (FUNC/FUNCP)
          WHENEVER.ABS.((ITT-IT(I,J,K))/ITT) .L. .02, TRANSFER TO AD
          IT(I,J,K) = ITT
AE        PRINT RESULTS F(I), T(J), VA(K), IT(I,J,K)
AD        IT(I,J,K) = ITT
          IEX(I,J,K)=ID(I,J,K) - IT(I,J,K)
AC        PRINT RESULTS F(I), T(J), VA(K), IT(I,J,K), IEX(I,J,K)
          WHENEVER DT .E.DS , TRANSFER TO XXX
          PRINT COMMENT $1PARTIALLY STRESSED, THERMAL, RS,DIODE ANALS
          AT = ( PI * DT * DT) / 4
          AS = (PI * DS * DS ) / 4
          FRAC = ( AT - AS)/ AT
          PRINT RESULTS DT, AT, DS, AS,  FRAC
          THROUGHAAAB,FOR I = 1,1, I .G. M
          THROUGHAAAB, FOR J = 1,1, J .G.N
          THROUGHAAAB, FOR K = 1,1, K.G. 20
          SI(I,J,K) = ID(I,J,K) - (    FRAC) * ID(1,J,K)
AAAB      PRINT RESULTS F(I), T(J),VA(K), SI(I,J,K)
          THROUGHAAAA , FOR I=1,1, I.G. M
          THROUGH AAAA , FOR J=1,1, J.G. N
          THROUGH AAAA,FOR  K=1,1, K.G. 20
AAAA      ID(I,J,K) = SI(I,J,K)
          DT = DS
          TRANSFER TO YYY
          END OF PROGRAM
```

REFERENCES

1-1 W. Schottky and W. Deutschman, Phys. Z. 30, 839 (1929).

1-2 F. Regler, Phys. Z. 31, 168 (1930).

1-3 W. Schottky, Naturwiss. 26, 843 (1938).

1-4 W. Schottky, Z. f. Phys., 113, 367 (1939).

1-5 A. L. Ward, Diamond Ordnance Fuze Laboratory Report, TR-731 (July 30, 1959).

1-6 W. Rindner, Am. Phys. Soc. 1, 65 (January 1962).

1-7 W. Rindner and I. Braun, Internal. Conf. Phys. Semicond., Exeter, 167 (1962).

1-8 W. Rindner and I. Barun, Bull. Am. Phys. Soc., 1, 331 (April 1962).

1-9 W. Rindner, J. Appl. Phys., 33, 2479 (1962).

1-10 J. J. Wortman, J. R. Hauser and R. M. Barger, J. Appl. Phys., 35, 2122 (1964).

2-1 J. Bardeen, Phys. Rev., 71, 717 (1947).

2-2 I. E. Tamm, Z. Phys., 76, 849 (1932).

2-3 W. Schockley, Phys. Rev., 56, 317 (1939).

2-4 C. A. Mead and W. G. Spitzer, Phys. Rev., 134, A 713 (1964).

2-5 C. A. Mead, Solid State Electronics, 9, 1023 (1966).

2-6 R. J. Archer et al., Phys. Rev. Lett., 12, 538 (1964).

2-7 A. M. Goodman, J. Appl. Phys., 35, 573 (1964).

2-8 A. M. Goodman, J. Appl. Phys., 36, 1411 (1965).

2-9 C. R. Crowell, J. C. Sorace, S. M. Sze, Trans. Metall. Soc., AIME, 233, 478 (1965).

2-10 J. Vanden Broek, Phillips Res. Rpts., 20, 624 (1965).

2-11 R. J. Archer and M. M. Atalla, N. Y. Acad. Sci., 101, 697 (1963).

2-12 See, for example, W. G. Dow, Fundamentals of Engineering Electronics, John Wiley and Son, New York (1952), p. 201.

2-13 H. K. Henisch, Rectifying Metal-Semiconductor Contacts, Clarendon Press, Oxford (1957), p. 199.

2-14 W. Shockley and W. T. Read, Jr., Phys. Rev., 87, 835 (1952).

2-15 R. N. Hall, Phys. Rev., 83, 228 (1951).

2-16 R. N. Hall, Phys. Rev., 87, 387 (1952).

2-17 C. Sah, R. N. Noyce and W. Shockley, Proc. IRE, 45, 1228 (1957).

2-18 J. R. Hauser, Proc. IEEE Corresp., 53, 743 (1965).

3-1 J. C. Phillips, Phys. Rev., 125, 1931 (1962).

3-2 W. P. Mason and T. B. Bateman, Phys. Rev., 134, A 1387 (1964).

3-3 J. Bardeen and W. Shockley, Phys. Rev., 80, 72 (1950).

3-4 C. Harring and E. Vogt, Phys. Rev., 101, 944 (1956).

3-5 W. H. Kleiner and L. M. Roth, Phys. Rev. Letters, 2, 334 (1959).

3-6 J. C. Hensel and H. Hasegawa, Proc. of 7th Internat. Conf. on Physics of Semiconductors, Paris 1964, Academic Press, 1964.

3-7 L. Kleinman, Phys. Rev., 128, 2614 (1962).

3-8 L. Kleinman, Phys. Rev., 130, 2283 (1963).

3-9 I. Goroff and L. Kleinman, Phys. Rev., 132, 1080 (1963).

3-10 J. J. Wortman, Ph. D. dissertation, Department of Electrical Engineering, Duke University (June, 1965).

3-11 W. P. Mason and T. B. Bateman, Phys. Rev. Lett., 10, 151 (1963).

3-12 P. Csavinsky and N. G. Einspruch, Phys. Rev., 132, 2434 (1963).

3-13 J. J. Wortman, J. R. Hauser, R. M. Burger, J. Appl. Phys., 35, 2122 (1964).

3-14 W. Shockley, Electrons and Holes in Semiconductors, Van Nostrand Co., Inc., Princeton (1950), p. 99.

3-15 Y. Matakura, Jap. J. Appl. Phys., 3, 256 (1964).

4-1 J. C. Hensel and H. Hasegawa, Proc. of 7th Internat. Conf. on Physics of Semiconductors, Paris 1964, Academic Press, 1964.

4-2 L. Kleinman, Phys. Rev., 128, 2614 (1962).

4-3 L. Kleinman, Phys. Rev., 130, 2283 (1963).

4-4 I. Goroff and L. Kleinman, Phys. Rev., 132, 1080 (1963).

4-5 D. Kahng, Solid State Electronics, 6, 281 (1963).

4-6 S. M. Sze, C. R. Crowell and D. Kahng, J. Appl. Phys., 35, 2534 (1964).

4-7 C. R. Crowell, S. M. Sze, W. G. Sitzer, Appl. Phys. Lett., 4, 91 (1964).

4-8 D. L. Scharfetler, Solid State Electronics, 8, 299 (1965).

4-9 R. J. Archer and M. M. Atalla, N. Y. Acad. Sci., 101, 697 (1963).

4-10 A. Many, Y. Goldstein, N. B. Grover, Semiconductor Surfaces, John Wiley and Sons, Inc., New York, 1965, p. 77.

4-11 Ibid. p. 357.

4-12 Integrated Circuits, ed. R. M. Warner, Jr. and J. N. Fordenwalt, McGraw-Hill Book Co., New York (1965), p. 306.

4-13 E. Fuchs, Phys. Z., 14, 1282 (1913).

4-14 S. Temoshenko and Goodier, Theory of Elasticity, McGraw-Hill Book Co., New York (1951), p. 377.

4-15 See, for example, J. Weertman and J. R. Weertman, Elementary Deslocktron Theory, The Macmillan Company, New York (1964).

4-16 W. Rindner (Private Correspondence).

4-17 H. Diamond (Private Correspondence).

5-1 J. J. Wortman, J. R. Hauser, R. M. Burger, J. Appl. Phys., 35, 2122 (1964).

A-1 J. F. Nye, Physical Properties of Crystals, Oxford University Press, London, 1957, pp. 82-105.

A-2 C. Kittel, Introduction to Solid State Physics, John Wiley and Sons, Inc., 1956, pp. 85-102.

A-3 W. P. Mason, Physical Acoustics and the Properties of Solids, D. Van Nostrand Co., Inc., 1958, Appendix A. 1.

A-4 P. M. Morse and H. Feshbach, Methods of Theoretical Physics, McGraw-Hill Book Co., Inc., 1953, Vol. 1, p. 25.

A-5 H. Goldstein, Classical Mechanics, Addison-Wesley Pub. Co., Inc., 1959, p. 95.

B-1 G. Bemski, Phys. Rev., 103, 567 (1956).